

NAVAL POSTGRADUATE SCHOOL

Monterey, California



THESIS

**DESIGN, DEVELOPMENT, AND TESTING OF AN
ULTRAVIOLET HYPERSPECTRAL IMAGER**

by

Erik O. Johnson

December, 1996

Thesis Advisors:

D. Cleary

S. Gnanalingam

Approved for public release; distribution is unlimited.

19970516 084

DTIC QUALITY INSPECTED 3

REPORT DOCUMENTATION PAGE			Form Approved OMB No. 0704-0188	
Public reporting burden for this collection of information is estimated to average 1 hour per response, including the time for reviewing instruction, searching existing data sources, gathering and maintaining the data needed, and completing and reviewing the collection of information. Send comments regarding this burden estimate or any other aspect of this collection of information, including suggestions for reducing this burden, to Washington Headquarters Services, Directorate for Information Operations and Reports, 1215 Jefferson Davis Highway, Suite 1204, Arlington, VA 22202-4302, and to the Office of Management and Budget, Paperwork Reduction Project (0704-0188) Washington DC 20503.				
1. AGENCY USE ONLY (Leave blank)		2. REPORT DATE December, 1996		3. REPORT TYPE AND DATES COVERED Master's Thesis
4. TITLE AND SUBTITLE DESIGN, DEVELOPMENT, AND TESTING OF AN ULTRAVIOLET HYPERSPECTRAL IMAGER (u)			5. FUNDING NUMBERS	
6. AUTHOR(S) Johnson, Erik O.				
7. PERFORMING ORGANIZATION NAME(S) AND ADDRESS(ES) Naval Postgraduate School Monterey CA 93943-5000			8. PERFORMING ORGANIZATION REPORT NUMBER	
9. SPONSORING/MONITORING AGENCY NAME(S) AND ADDRESS(ES)			10. SPONSORING/MONITORING AGENCY REPORT NUMBER	
11. SUPPLEMENTARY NOTES The views expressed in this thesis are those of the author and do not reflect the official policy or position of the Department of Defense or the U.S. Government.				
12a. DISTRIBUTION/AVAILABILITY STATEMENT Approved for public release; distribution is unlimited.			12b. DISTRIBUTION CODE	
13. ABSTRACT (maximum 200 words) This research involved the development of an ultraviolet (UV) hyperspectral imager. A hyperspectral image is a three dimensional image in which two of the dimensions provide spatial information and the third provides spectral information. In an effort to minimize the cost of this experiment, the NPS Middle Ultraviolet SpecTrograph for Analysis of Nitrogen Gases (MUSTANG) instrument was modified to function as a hyperspectral imager. This required the design, fabrication, and testing of hardware and software to coordinate the operation of a two dimensional, charge coupled device (CCD) detector with a servo-controlled scanning mirror. Control and synchronization of scanning mirror and image collection was accomplished by software (written in Borland C++) run from an Intel microprocessor based PC. The benefits of a UV hyperspectral imager are primarily in the area of Support to Military Operations (SMO). There are two principal applications: 1) target identification, and 2) battle damage assessment. Additionally, this instrument has dual use applications, namely, 1) redirection of jet aircraft to avoid the foreign object damage (FOD) hazards presented by volcanic ash clouds through analysis of the absorption of solar UV radiation by the sulfur dioxide (SO ₂) gas associated with volcanic ash, and 2) forest fire detection.				
14. SUBJECT TERMS Hyperspectral Imaging, Ultraviolet, Imaging Spectroscopy, Remote Sensing, Dual Use, Support to Military Operations			15. NUMBER OF PAGES 70	
			16. PRICE CODE	
17. SECURITY CLASSIFICATION OF REPORT Unclassified	18. SECURITY CLASSIFICATION OF THIS PAGE Unclassified	19. SECURITY CLASSIFICATION OF ABSTRACT Unclassified	20. LIMITATION OF ABSTRACT UL	

NSN 7540-01-280-5500 Standard Form 298 (Rev. 2-89)

Prescribed by ANSI Std. Z39-18 298-102

Approved for public release; distribution is unlimited.

**DESIGN, DEVELOPMENT, AND TESTING OF AN ULTRAVIOLET
HYPERSPSPECTRAL IMAGER**

Erik O. Johnson
Lieutenant, United States Navy
B.S., University of La Verne, California, 1988


Submitted in partial fulfillment
of the requirements for the degree of

MASTER OF SCIENCE IN APPLIED PHYSICS

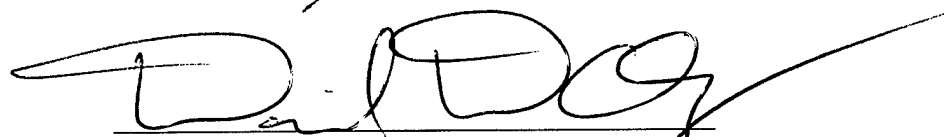
from the

**NAVAL POSTGRADUATE SCHOOL
December 1996**

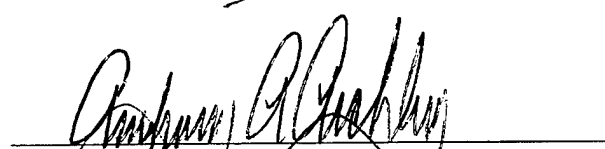
Author:


Erik O. Johnson

Approved by:


David D. Cleary, Thesis Advisor


S. Gnanalingam, Second Reader


Anthony A. Atchley, Chairman
Department of Physics

DTIC QUALITY INSPECTED 8

ABSTRACT

This research involved the development of an ultraviolet (UV) hyperspectral imager. A hyperspectral image is a three dimensional image in which two of the dimensions provide spatial information and the third provides spectral information. In an effort to minimize the cost of this experiment, the NPS Middle Ultraviolet SpecTrograph for Analysis of Nitrogen Gases (MUSTANG) instrument was modified to function as a hyperspectral imager. This required the design, fabrication, and testing of hardware and software to coordinate the operation of a two dimensional, charge coupled device (CCD) detector with a servo-controlled scanning mirror. Control and synchronization of scanning mirror and image collection was accomplished by software (written in Borland C++) run from an Intel microprocessor based PC. The benefits of a UV hyperspectral imager are primarily in the area of Support to Military Operations (SMO). There are two principal applications: 1) target identification, and 2) battle damage assessment. Additionally, this instrument has dual use applications, namely, 1) redirection of jet aircraft to avoid the foreign object damage (FOD) hazards presented by volcanic ash clouds through analysis of the absorption of solar UV radiation by the sulfur dioxide (SO_2) gas associated with volcanic ash, and 2) forest fire detection.

TABLE OF CONTENTS

I. INTRODUCTION	1
A. OBJECTIVES	3
B. THESIS OUTLINE	3
II. BACKGROUND	5
A. REMOTE SENSING	5
B. HYPERSPECTRAL IMAGERY	6
C. MOTIVATION FOR A UV IMAGING SPECTROGRAPH	8
D. MUSTANG DESCRIPTION	10
III. MUSTANG CONVERSION	13
A. GRATING SELECTION	14
B. DETECTOR UPGRADE	17
C. SCANNING MIRROR INSTALLATION	26
D. SOFTWARE DEVELOPMENT	33
IV. DATA COLLECTION	39
V. CONCLUSION	45
A. SUMMARY OF FINDINGS	45
B. RECOMMENDATION FOR FURTHER RESEARCH	45
APPENDIX	49
LIST OF REFERENCES	57
INITIAL DISTRIBUTION LIST	59

LIST OF ABBREVIATIONS

AMI	All-Reflection Michelson Interferometer
AVIRIS	Airborne Visible/Infrared Imaging Spectrometer
CCD	Charge Coupled Device
COTS	Commercial Off The Shelf
CsTe	Cesium Telluride
DUUVIS	Dual Use UltraViolet Imaging Spectrograph
EDD	Electronic Digital Driver
FOV	Field Of View
FUV	Far Ultraviolet
Hg	Mercury
IDL	Interactive Data Language
IFOV	Instantaneous Field Of View
LSB	Least Significant Bit
MCP	Microchannel Plate
MgF ₂	Magnesium Fluoride
MOS	Metal Oxide Semiconductor
MSB	Most Significant Bit
MTF	Modulation Transfer Function
MUSTANG	Middle Ultraviolet SpecTrograph for Analysis of Nitrogen Gases
MUV	Middle Ultraviolet
NPS	Naval Postgraduate School
NUV	Near Ultraviolet
OPD	Optical Path Difference
PSF	Point Spread Function
Pt	Platinum
TIFF	Tagged Image File Format
UAV	Unmanned Aerial Vehicle
UV	Ultraviolet

I. INTRODUCTION

Over the past decade, advancements in remote sensors have led to an effective technique for image data acquisition, namely, Hyperspectral Imagery (HSI). The HSI process is a form of "imaging spectrometry" in which an image is obtained at many contiguous wavelengths (100 or more spectral bands) with spectral resolution sufficient to distinguish features of interest (e.g. molecular transitions in materials with spectral resolution on the order of 1 - 2 nm). This technique generates a three dimensional image in which two of the dimensions contain spatial information and the third dimension contains spectral information. To date, some 45 hyperspectral sensor systems are either deployed or under development. Most of these sensors detect radiation in the visible or far infra-red (400 nm - 15 μ m) portions of the electromagnetic spectrum, and only 2 of them detect radiation below 400 nm. This research involved the design, fabrication, and testing of the first mid ultraviolet (MUV) hyperspectral imager built to operate in the MUV to visible (200 - 500 nm) region of the electromagnetic spectrum. This ultraviolet (UV) imager will extend the range of current hyperspectral imagers and enhance existing capabilities for exploiting the spectral signature of targets.

The UV spectrum can be divided into three regions, namely, the far ultraviolet (FUV) (100 - 200 nm), MUV (200 - 300 nm), and near ultraviolet (NUV) (300 - 400 nm). Atmospheric transmission of radiation in the troposphere in both the middle and near UV regions, is mainly determined by scattering (Rayleigh and Mie). Transmissivity in these two regions is relatively high for path lengths up to tens of kilometers, depending on wavelength. In the stratosphere, absorption by molecular oxygen can result in complete extinction of radiation in the FUV over a distance of less than ten meters, again depending on wavelength. Since our applications involve remote sensing, this transmissive property of radiation in the FUV caused us to restrict the lower end of our instrument bandwidth to the MUV.

In the NUV, solar radiation penetrates the earth's atmosphere providing natural illumination. Radiation in this wavelength region is similar to visible light in that target materials are identified by their reflectance spectrum. Although both the target and

background can be relatively bright at these wavelengths, many materials experience electronic transitions in this region. The advantage of operating in the NUV is that each transition observed aides in the unique identification of a specific material.

Most of the solar radiation in the MUV region, is prevented from reaching the Earth's surface by the ozone layer at an altitude of 40 km. A MUV sensor operating at an altitude below the ozone layer, would observe almost zero natural background illumination. Propagation of any MUV radiation existing between the ground and the ozone layer can still be appreciable. The combined effects of the ozone layer and favorable atmospheric transmission below it, allow for detection of weak target signatures emanating from artificial sources of MUV radiation with an extremely low probability of false alarm. For example, fluorescent lights are common in nearly all buildings and structures. These lamps have a number of atomic Mercury emissions in the Middle UV. It is possible that the scattering of this radiation near building openings such as doors or windows, could be used for overhead detection of human activity, or even battle damage assessment (BDA).

The interest in the blue-green (400 - 500 nm) region of the visible spectrum is due to it's favorable transmission properties in water. **Figure 1** shows that light with wavelengths between 380 and 500 nm have the lowest coefficients for both absorption

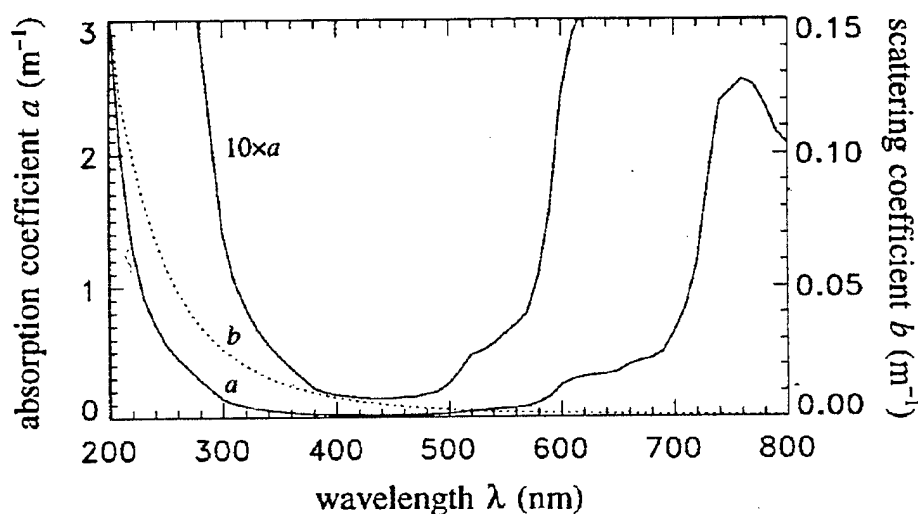


Figure 1: Absorption and Scattering Coefficients vs. Wavelength for Transmission in Pure Sea Water. Taken From Mobley (1994).

and scattering in pure sea water. This is extremely beneficial in the area of submarine and mine detection in littoral waters.

To briefly recap, the new NPS Mid Uv hyperspectral imager would have a bandwidth covering three principal regions with the following utilities:

1. Mid Uv - overhead detection of human activity/BDA.
2. Near UV - observation of electronic transitions to aide in the unique identification of specific materials.
3. Short-wave Visible - submarine/mine detection in littoral waters.

A. OBJECTIVES

The objectives of the research described in this thesis were to design, fabricate, and test the first Mid Uv hyperspectral imager. Design of the instrument was driven by two principal factors, namely, economy and size. Limited funding resources encouraged maximum utilization of existing components. Thus, the NPS Middle Ultraviolet SpecTrograph for Analysis of Nitrogen Gases (MUSTANG) instrument was chosen to be the backbone of the new design. Furthermore, additional components required for MUSTANG's conversion were selected from commercial off the shelf (COTS) items. The size limit was imposed by the ultimate goal of flying the instrument aboard one of the NPS Unmanned Aerial Vehicles (UAV)'s during subsequent research.

B. THESIS OUTLINE

This thesis is divided into five chapters and one appendix. The first chapter is the introduction. Chapter two provides the background information for the design and development of the NPS UV hyperspectral imager. These areas include an overview of hyperspectral imagery and the NPS MUSTANG instrument. Details of the conversion of MUSTANG into a UV hyperspectral imager are provided in chapter three. Chapter four discusses the data collected by the new hyperspectral instrument. Conclusions and recommendations for future design improvements are contained in Chapter five. The goal of this work was to demonstrate the operation of the first UV hyperspectral imager by generating the first UV hypercube. One appendix is included which contains a listing of the instrument control and data collection programs.

II. BACKGROUND

This chapter provides a brief introduction to remote sensing and the progression from early imaging techniques to hyperspectral imaging. Additionally, it uses an example to provide motivation for development of a UV imaging spectrograph. Finally, it introduces the MUSTANG instrument which will be thoroughly investigated in follow-on chapters.

A. REMOTE SENSING

It is often easier to observe measurable features of an item of interest from a considerable distance rather than close-up. For example, it is easier to construct a map of a valley from an observation point high atop a mountain than from within the valley itself. In the early days of remote sensing, cameras were mounted on balloons (and even kites) to obtain aerial photographs of the land below. The information gained from these photos proved extremely useful in a variety of applications ranging from locating armies to surveying unexplored territories. The once mysterious Amazon River and it's surrounding rain forest which was impervious to the advance of civilization, is now charted and open for development as a result of aerial surveying. As technology improved, airplanes and satellites served as the host platforms for the sensing equipment. Just as the host platforms improved, so did the sensors.

The earliest remote sensing images were black and white photographs. These were bi-spectral in nature, that is, distinguishing features of an object were depicted by varying shades of gray resulting from different combinations of black and white. Information obtained through literal interpretation of these black and white images was somewhat limited. This is because the human eye is a multi-spectral sensor which allows us to recognize a multitude of colors through combinations of three spectral bands, namely, red, green and blue. Unfortunately, this remarkable color sensor is rather limited in its resolution of shades of gray. At best, a trained analyst can only distinguish about ten. Since the initial data obtained from remote sensors was in the form of photographs

which were interpreted by trained human analysts, it was a natural progression to develop multi-spectral sensors.

Color images obtained from early multi-spectral sensors provided much more information than their black and white predecessors. The next logical progression was to extend the sensor's range beyond the visible spectrum into the UV and infrared (IR). Today's multi-spectral sensors have on order of 10 spectral bands which sample the electromagnetic spectrum at various points between the UV and IR regions. These are considered to be broad band sensors since their spectral bands (or channels) are fairly wide, ranging from a few tenths of a micron up to several microns. Images generated from spectral bands outside the visible region can no longer be literally interpreted. Since the human eye is incapable of viewing UV or IR radiation, false coloring must be applied to data from those spectral channels. Additionally, there are many algorithms which employ techniques of linear algebra to perform transformations on the data in different multi-spectral bands to enhance their signal to noise ratio. Various combinations of the bands are then examined until the characteristic of interest is exploited.

In addition to providing more information, increasing the number of spectral bands opened the door to an even greater range of applications such as terrestrial land ecology, bathymetry, and geology. Green plants, for example, use chlorophyll to absorb the visible light from the sun, but reflect radiation in the Near IR ($0.7\text{ }\mu\text{m}$ - $2.5\text{ }\mu\text{m}$). Sensors operating in this bandwidth will record a significant increase in reflectance around $0.7\text{ }\mu\text{m}$ due to the presence of vegetation. Incidentally, a military application of this same phenomenon is detection of camouflaged objects such as artillery installations, tanks, and troops. Today, there are IR reflecting camouflage paints capable of deceiving broad band multi-spectral sensors. However, these paints each have unique spectral signatures which could be exploited by an imaging spectrometer. Hyperspectral imagers were designed with this type of application in mind.

B. HYPERSPECTRAL IMAGERY

As previously mentioned, hyperspectral imagers split a portion of the electromagnetic spectrum into many distinct, contiguous, narrow channels whose widths

are on the order of a few nanometers or less. This allows for very precise spectral signature discrimination which broad band multi-spectral imagers are incapable of providing. Exactly which method is employed for conducting such a precise spectral signature analysis is the basis of a great deal of ongoing research. The general consensus is that literal interpretation of remote sensing imagery by trained human analysts is a thing of the past. This is not necessarily bad since human interpretations are highly subjective and not perfectly repeatable. Hyperspectral images contain a vast amount of precision data which lends itself rather nicely to digital processing. An appreciation of the amount of information collected by a hyperspectral imager can be gained from the hyperspectral cube provided in **Figure 2**. This image was produced by Jet Propulsion Laboratory's Airborne Visible Infra-Red Imaging Spectrometer (AVIRIS) instrument during an August 20, 1992 overflight of Moffett Field on a NASA ER-2 plane at an

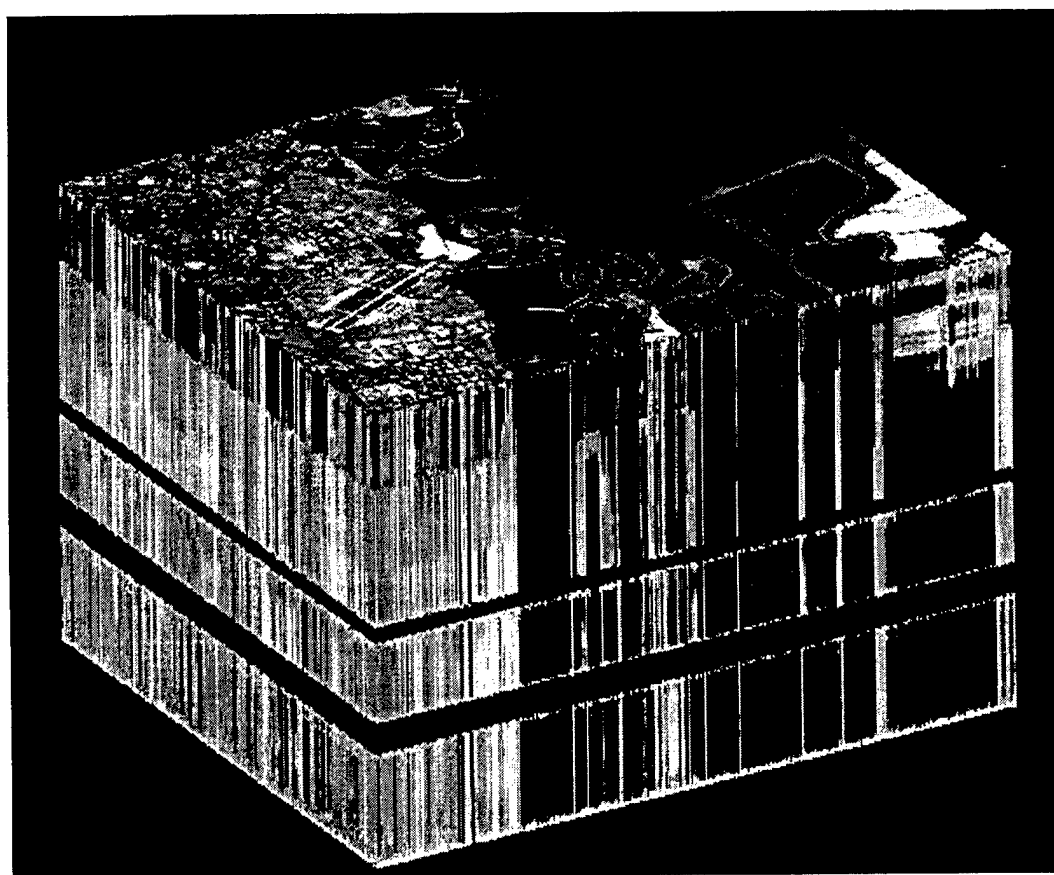


Figure 2: AVIRIS "Hypercube", Taken From JPL (1994).

altitude of 20 km (65,000 ft). Although the hypercube is not a desirable format for data analysis, it clearly illustrates the nature of a hyperspectral image. Two dimensional spatial information is contained in the x-y plane (i.e. the top of the cube), and spectral information is contained in the z direction. AVIRIS has 224 spectral channels ranging from 400 nm to 2.5 μm . In Figure 2, spectral information is ordered such that the shortest wavelength is at the top of the cube and the longest wavelength at the bottom. The two solid dark lines traversing the lower half of the cube represent the absorption of IR at 1.4 μm and 1.9 μm due to the presence of water molecules in the atmosphere. Note the rectangular features located in the upper right corner of the cube's larger side. They represent a marked response in the red portion of the visible spectrum (around 700 nm) to the presence of one centimeter long brine shrimp residing in an evaporation pond located in the far right corner of the top of the cube. The ability to identify such minute features from an altitude of 65,000 feet boggles the mind, however, this is only the tip of the iceberg regarding potential capability of a rapidly evolving technology.

C. MOTIVATION FOR A UV IMAGING SPECTROGRAPH

Figure 3 illustrates the vast amount of volcanic ash introduced into the atmosphere as a result of volcanic eruption during recent activity beneath Vatnajökull glacier in Iceland. While the eruption poses an immediate threat to nearby land inhabitants, it also commands the respect of aviators as the ash cloud presents a Foreign Object Damage (FOD) hazard to gas turbine engines. Current procedure is to give the ash cloud an extremely wide berth (sometimes entire continents are avoided). Large savings in time and money could be achieved through the accurate identification (or prediction) of the "safe" ash cloud perimeter.

In addition to the lava, ash, etc., one of the products of a volcanic eruption is SO_2 . In fact, a strong correlation exists between the presence of volcanic ash and the concentration of SO_2 . This is evidenced by the data obtained from the Total Ozone Mapping Spectrometer (TOMS), an instrument on board the Nimbus-7 low earth orbiting satellite [Krueger et. al., 1995]. Nimbus-7 is in a polar sun-synchronous orbit. That is, it crosses the equator every 26 degrees of longitude at local noon, making approximately



Figure 3: October '96 Eruption Beneath Vatnajökull Glacier in Iceland. Taken From the Nordic Volcanological Institute (1996).

13.7 orbits/day, thus observing the entire earth once a day. TOMS is a multi-spectral instrument with six spectral bands ranging from 312 nm - 380 nm originally designed to monitor ozone depletion by measuring the ratio of back-scattered Earth radiance to incoming solar irradiance representative of UV absorption by the ozone layer. As a result of TOMS contiguous spatial mapping of the earth in the Near UV, it recorded strong absorptions in its shortest wavelengths due to SO_2 in the volcanic plume during the 1982 El Chichon eruption [Krueger et. al., 1995]. Since then, TOMS has been monitoring SO_2 with its four shorter spectral bands (312.5, 317.5, 331.2, and 339.8 nm) to provide a continuous record of volcanism.

In the previous chapter, the NPS UV imaging spectrograph was proposed as a dual use instrument, meaning that it could support commercial applications in addition to its support to military operations. Providing accurate identification of safe ash cloud perimeters for civilian aircraft as a result of SO_2 analysis is a prime example of such an application. A strong portion of the SO_2 absorption spectrum extends down to 260 nm, see **Figure 4** below. This is well below the minimum detectable wavelength of the TOMS instrument. Additionally, there is an overlap of the SO_2 absorption spectrum with the absorption systems of both ozone (300 nm - 360 nm) and sulfur monoxide (SO) (250 nm - 285 nm) which is difficult to discern with a multi-spectral instrument. A hyperspectral imaging system is necessary in this situation to properly sort things out. Additionally, the proposed NPS instrument is capable of actually being flown through an ash cloud in an experiment designed to provide an accurate assessment of the exact correlation between SO_2 concentration and volcanic ash concentration.

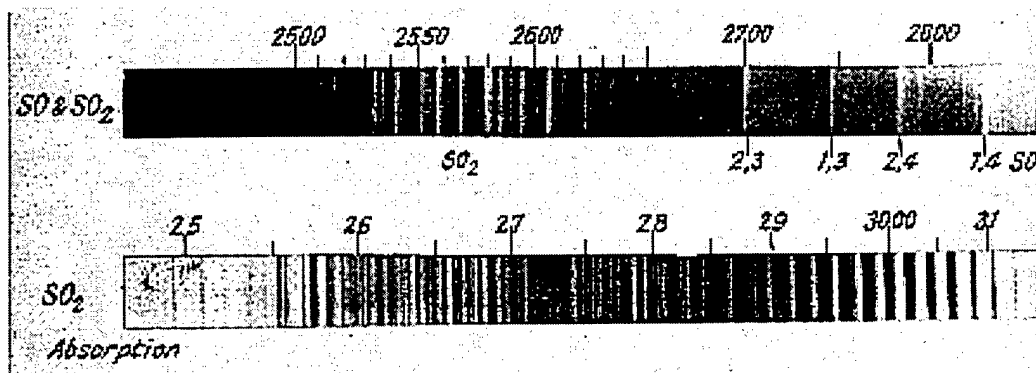


Figure 4: SO and SO_2 Absorption Lines. Taken From Pearse and Gaydon (1963).

D. MUSTANG DESCRIPTION

The NPS MUSTANG instrument is a 1/8th m Ebert-Fastie spectrograph which has been flown on three separate NASA sounding rocket experiments to obtain information on nitrogen gases in the ionosphere. MUSTANG's major components are illustrated in **Figure 5**. Incident light enters the off-axis telescope where it is collimated by a series of baffles prior to striking a 1/8th m spherical mirror. Reflected light from the telescope mirror is focused onto a 5mm by 140 μm vertical slit. After passing through

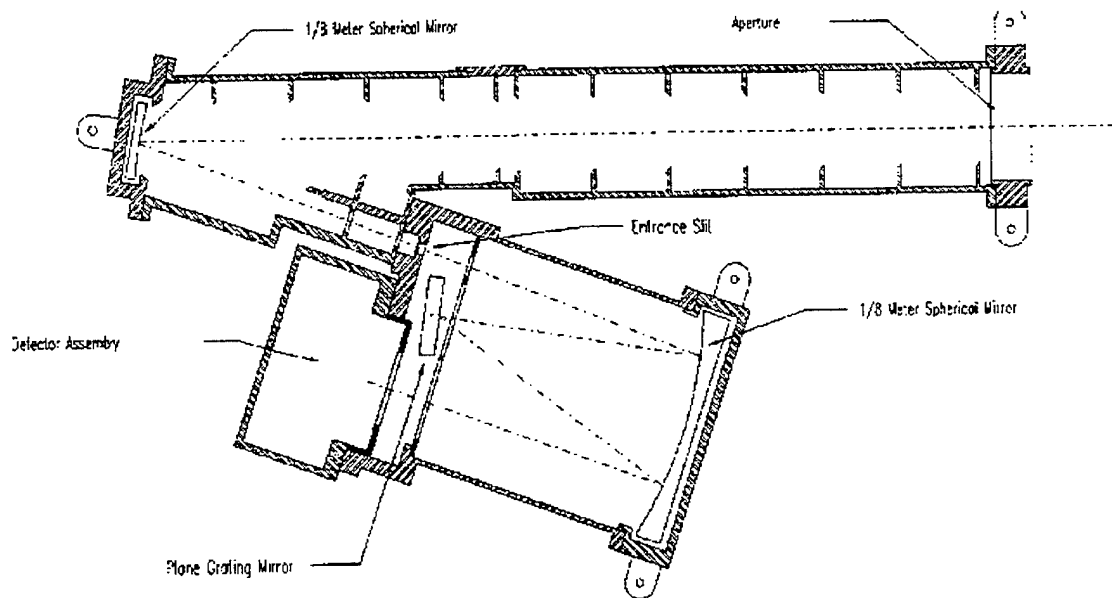


Figure 5: MUSTANG Instrument. Taken From Atkinson (1993).

the entrance slit, the light is reflected off the 1/8 m Ebert mirror onto a reflective, plane diffraction grating. The grating separates the incident polychromatic light into its monochromatic components which are directed back to the Ebert mirror and subsequently focused onto the detector area in the exit focal plane. The instrument's original detector was a one dimensional Plasma-Coupled Device (PCD), a monolithic, self scanning linear array of 512 p-n junction photodiodes. MUSTANG's output was in the form of a plot of intensity vs. wavelength. A typical spectrum of the instrument is shown in **Figure 6**.

With a 1200 ruling per mm grating and a 25mm detector aperture, MUSTANG had a band pass of 135 nm at a spectral resolution of approximately 1 nm [Cleary et. al., 1995]. MUSTANG's spectrograph provided 135 narrow spectral channels which would be ideal for hyperspectral imagery if the instrument could be modified to produce a two dimensional image.

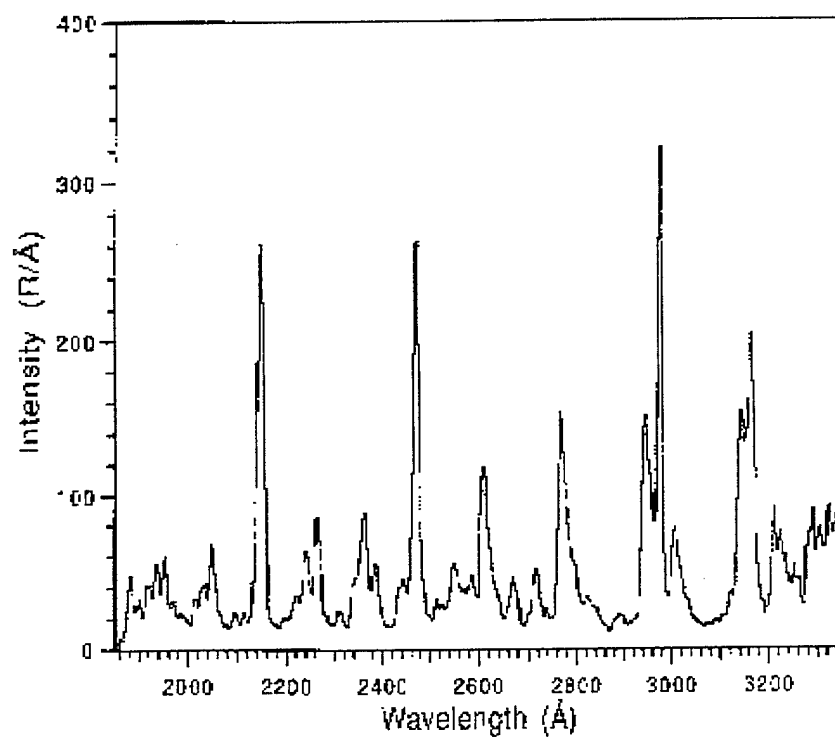


Figure 6: Typical Spectrum from MUSTANG Instrument. Taken From Hymas (1994).

III. MUSTANG CONVERSION

In an effort to minimize the cost of developing the NPS hyperspectral imager, the decision was made to modify the existing MUSTANG instrument to enable it to function as an imaging spectrograph. Additionally, the stipulation was made that any new piece of hardware purchased for the conversion had to be a COTS item. Simply stated, the basic approach to the problem was to retrofit MUSTANG with a two dimensional detector and install a scanning mirror at the entrance of the telescope. Since both focal length and entrance slit would remain unchanged, the new instrument, DUUVIS (Dual Use Ultra-Violet Imaging Spectrograph) would have the same instantaneous field of view (IFOV) as MUSTANG, namely, 2.3° in the vertical direction and 0.06° in the horizontal direction. At any given instant of time, a "snapshot" taken with DUUVIS would produce a very narrow sliver of a hyperspectral image. As illustrated in **Figure 7** below, each "sliver" contains spatial information in the y-direction and spectral information (from 135 narrow channels) in the z-direction. Once a snapshot is stored, the scanning mirror is repositioned to obtain the next adjacent sliver and the process is repeated. After the mirror has scanned through the entire field of view (FOV), all the slivers are combined into one image file and the instrument is ready to begin all over again. The transformation of MUSTANG into DUUVIS was comprised of four main elements:

1. Grating selection
2. Detector upgrade

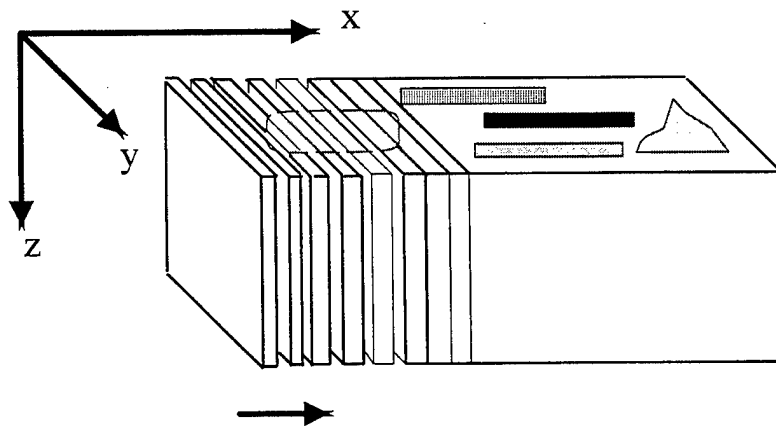


Figure 7: Method of Constructing a Hyperspectral Image with DUUVIS Data.

3. Scanning mirror installation
4. Software development.

This chapter will elaborate on each of the aforementioned elements.

A. GRATING SELECTION

As previously mentioned, DUUVIS is designed to operate in the Mid UV through visible portion of the electromagnetic spectrum. Unfortunately, it is not possible for the instrument to cover the entire spectral range from 200 nm through 500 nm simultaneously and maintain the desired spectral resolution. A sketch of the optical path through the spectrograph is provided in **Figure 8**. The spectrograph is configured such that the incident angle between the incoming light and the normal of the grating is 9.1° when $\phi = 0$. The instrument bandpass is a function of the separation distance between rulings on the grating and the detector aperture. Detector position dictates that the minimum detectable wavelength is that which has an exit angle of approximately 10° and the maximum detectable wavelength is that which has an exit angle of 20° . Rotating the grating so that it is no longer normal to the Ebert mirror causes the values of the minimum and maximum detectable wavelengths to change. However, the width of the bandpass remains roughly constant. A more detailed description of this relationship is

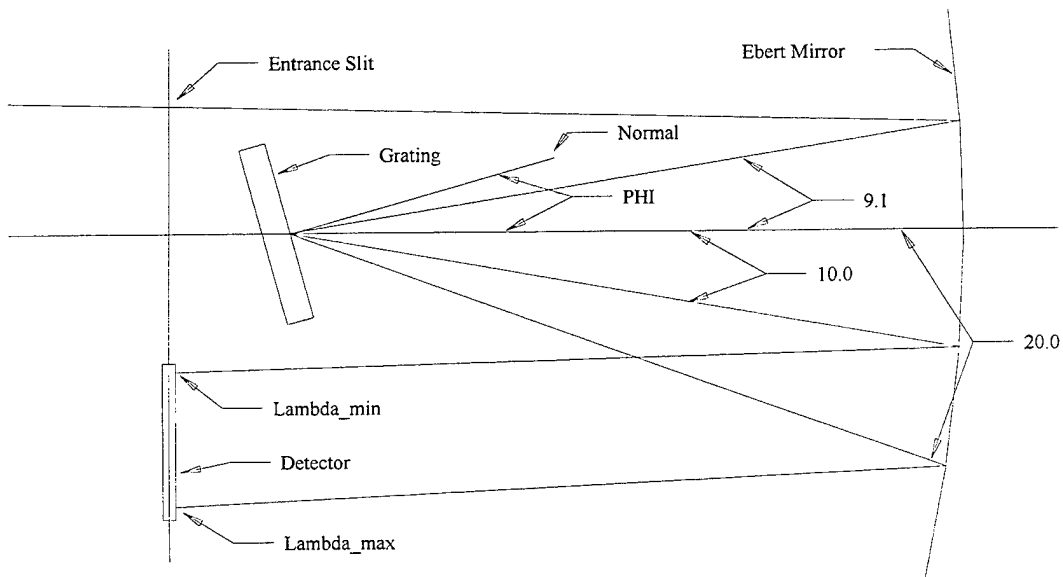


Figure 8: Optical Path Through DUUVIS Spectrograph.

provided below. Since the focal length of our instrument is much greater than the separation distance between the rulings, we assume the light rays to be parallel in both the incident and diffracted wavefronts. As illustrated in **Figure 9**, the total difference in path length between two incident rays of light after reflecting off adjacent rulings in the grating is given by $d \sin \alpha + d \sin \beta$, where d is the separation distance between rulings, α is the incident angle, and β is the exit angle. When this difference in path length is equal to an integral multiple, n , of the wavelength of interest, the reflected rays will be in phase and produce a spectral line of order n . At all other angles, there is some measure of destructive interference. Therefore, the diffracted beams will only exist at the angles β_n as prescribed by the grating equation:

$$n\lambda = d \sin \alpha - d \sin \beta_n,$$

where: n = order number of the spectral line of interest.
 λ = wavelength of the spectral line of interest.
 α = Incident angle of the incoming light onto the grating.
 β_n = Exit angle of spectral line of interest.

It was previously stated that rotation of the grating determined the minimum detectable wavelength. How is that grating angle determined? Suppose we rotate the

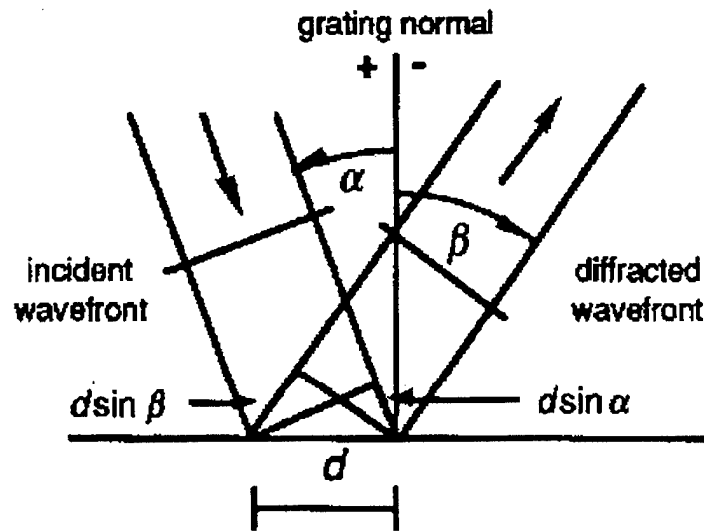


Figure 9: Geometry of Diffraction. Taken From Milton Roy Company (1994).

grating so that it's normal is displaced by an angle ϕ while keeping α constant. We define α to be the incident angle of the incoming light with respect to the optical axis of the Ebert mirror, then $\theta'_i = \phi - \alpha$ represents the incident angle, and $\theta'_e = \phi + \alpha$ the exit angle. The grating equation becomes:

$$n\lambda = d \sin \theta'_i + d \sin \theta'_e = d[\sin(\phi - \alpha) + \sin(\phi + \alpha)],$$

substituting the proper trigonometric identities ...

$$n\lambda = d[(\sin \phi \cos \alpha - \cos \phi \sin \alpha) + (\sin \phi \cos \alpha + \cos \phi \sin \alpha)],$$

$$n\lambda = d(2 \sin \phi \cos \alpha), \text{ solving for } \phi \text{ we arrive at } \phi = \sin^{-1} \left[\frac{n\lambda}{2d \cos \alpha} \right].$$

Since this is an Ebert monochromator, we are dealing with first order spectra therefore $n = 1$. In our instrument, α is fixed at 9.1014° , thus we can determine the grating angle ϕ necessary to obtain the desired minimum detectable wavelength from:

$$\phi = \sin^{-1} \left[(0.5064) \frac{\lambda}{d} \right].$$

Once ϕ is known, it can be substituted back into the grating equation to find the values for the corresponding minimum and maximum detectable wavelengths. For example, with a 1200 line/mm grating at an angle of 6.3° , $\lambda_{\min} = 193 \text{ nm}$, $\lambda_{\max} = 328 \text{ nm}$, and the instrument bandpass is 135 nm. A significant increase in bandpass can be achieved by installing a 600 line/mm grating. Setting the grating angle at 3.0° , we obtain $\lambda_{\min} = 200 \text{ nm}$, $\lambda_{\max} = 476 \text{ nm}$, with an instrument bandpass of 276 nm. This increase in bandpass does not come without cost. Spectral resolution is controlled primarily by the instrument dispersion and entrance slit width. Instrument dispersion is controlled by, among other things, the grating ruling density. Reducing the number of rulings by a factor of two causes a reduction in resolution by a factor of two as well. There are three plane diffraction gratings currently available for DUUVIS, these include, 600 l/mm, 1200 l/mm, and 2400 l/mm. This grating assortment allows for extreme flexibility in tailoring the instrument to a variety of applications. **Table 1** provides a summary of capabilities based on grating ruling density. Note that the bandpass and resolution are subject to

change while the number of spectral channels (bandpass/resolution) remains fairly constant.

Two gratings were utilized during this experiment, one had 1200 lines/mm and the other, 600 lines/mm. The 1200 l/mm grating has a bandpass and resolution which match well with the challenges of SO₂ analysis while the 600 l/mm is better suited for rocket plume analysis.

Table 1. Summary of Capabilities

Grating Density (l/mm)	Instrument Bandpass (nm)	Resolution (nm)
7,600	276	2
1,200	135	1
2,400	64	0.5

B. DETECTOR UPGRADE

The next step in MUSTANG's conversion was replacement of it's one-dimensional PCD detector with a two-dimensional detector. Adhering to the economical restrictions described earlier, the decision was made to adopt a detector which was already employed in the NPS All-Reflection Michelson Interferometer (AMI) [Hicks 1995]. This detector is contained in a high resolution digital camera (the EDC-1000HR) produced by the Electrim Corporation and commercially available for under \$1000.00. This created two major challenges: 1) The necessity to marry products from the spectroscopy community (one inch wide rectangular standard aperture) with those from the photography community in which circular apertures are standard, and 2) Ensuring that design requirements met the needs of both DUUVIS and AMI while maintaining complete interchangeability between the two instruments.

The detector is a charge coupled device (CCD) which is sensitive to visible light at wavelengths between 400 nm - 1100 nm. Since we're interested in wavelengths between 200 nm and 400 nm, modifications were necessary to convert the incident UV light into visible light for the CCD. A commercially available Image Intensifier Tube (IIT) performs that task quite nicely. The image intensifier is a proximity focused channel intensifier tube with dual microchannel plates. It was manufactured by BV Delft Electronische Producten (DEP) located in Holland. The basic intensifier consists of a

quartz input window, a photocathode, two microchannel plates, a phosphor screen and a fiber-optic face plate for output. A quartz window is used to allow UV light to enter the detector since glass is opaque at Mid UV wavelengths. Incident light encounters an S-20 photocathode which converts incident photons into electrons. S-20, the name of the coating on the photocathode, is made from a multi-alkalide compound known as Suprasil which, among others, contains cesium, potassium, sodium and antimony. The S-20 photocathode is sensitive to light with wavelengths between 200 nm and 520 nm. Primary electrons emitted by the photocathode are directed to the microchannel plate (MCP) assembly. **Figure 10** is an illustration of a microchannel plate.

The MCP is comprised of millions of glass capillaries (channels) with an inner diameter of approximately ten μm . Each tube acts as an independent photo-multiplier. An electric potential (+6000 Vdc) is established across the MCP as seen in **Figure 11**. Incident primary electrons collide with the capillary walls and strip off electrons from the glass in the process. These secondary electrons are accelerated by the difference in electrical potential across the MCP. Accelerated secondary electrons collide with the capillary walls and strip off more electrons, etc.. This cascading of electrons results in approximately 15,000 electrons at the output of the MCP for every single electron emitted by the photocathode. The amplified electron beam is subsequently focused onto an aluminum screen coated with P-43 luminescent phosphor causing it to fluoresce

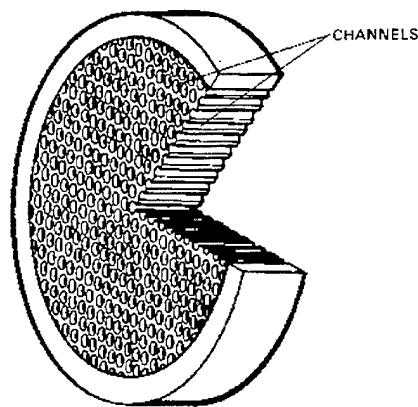


Figure 10: MCP Construction. Taken From Hamamatsu Photonics (1985).

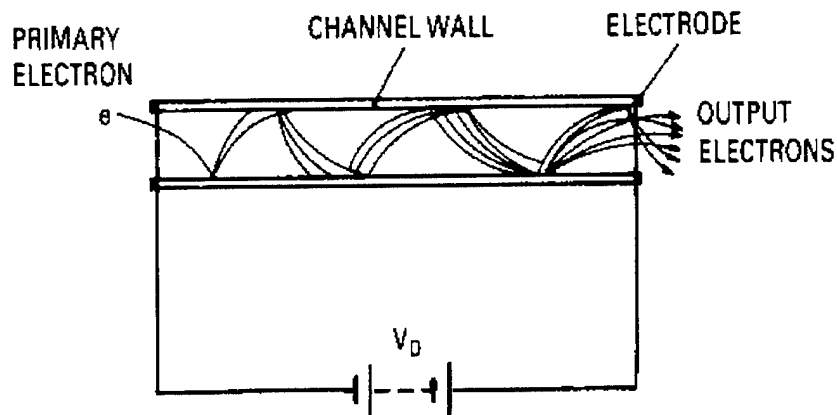


Figure 11: Electric Representation of Electron Amplification. Taken From Hamamatsu Photonics (1985).

thereby emitting photons with wavelengths between 535 nm to 555 nm. Photons are then directed to the output of the IIT via a 25 millimeter diameter fiber-optic faceplate which preserves the spatial order of the image. The incident UV light is thus converted into visible light within the CCD's sensitivity range.

The CCD utilized in the digital camera is a TI-241 chip, manufactured by Texas Instruments, which consists of a two dimensional array (753(H) x 244(V) pixels) of closely spaced metal oxide semiconductor (MOS) capacitors. Incident photons have energies which exceed the bandgap energy of the silicon material of the MOS capacitor. This causes them to be absorbed by the semiconductor material resulting in the formation of an electron-hole pair. Electrons are collected in energy wells generated by each of the MOS capacitors when their gates are positively biased (i.e. during the integration portion of the operation cycle). The amount of charge collected in each of these "packets" is proportional to the total integrated light flux incident upon an individual MOS capacitor during the measurement period [Wilson and Hawkes, 1989]. "Read out" of the charge packets is accomplished by sequentially reversing the bias on the capacitors thereby transferring the stored charge from the image columns (exposed to incident radiation) to the vertical shift registers which are shielded from incident radiation. During the scan period, each charge packet is sequentially transferred from the vertical shift registers to

the horizontal shift (readout) register to be processed by the computer as shown in **Figure 12**. Using an analog-to-digital (A/D) converter, the output is transformed into an 8 bit signal and is used for display or storage in a tagged image file format (TIFF) file for further analysis.

MUSTANG had a circular aperture IIT very similar to the one previously described. However, the one dimensional nature of it's detector did not require any further optical consideration. The 25 mm diameter of the IIT matched quite well with the one inch horizontal width of the linear array allowing the fiberoptic output window of the IIT to be directly mated to the face of the PCD detector. In the case of DUUVIS, it became necessary to focus the two dimensional image produced by the 25 mm dia. circular aperture IIT down onto the 8.67 mm by 6.59 mm rectangular sensing area of the CCD. In the initial AMI configuration, a high quality fiber-optic taper with a demagnification ratio of 1.6 is used to transfer the image to the 11 millimeter cross-diagonal face plate of

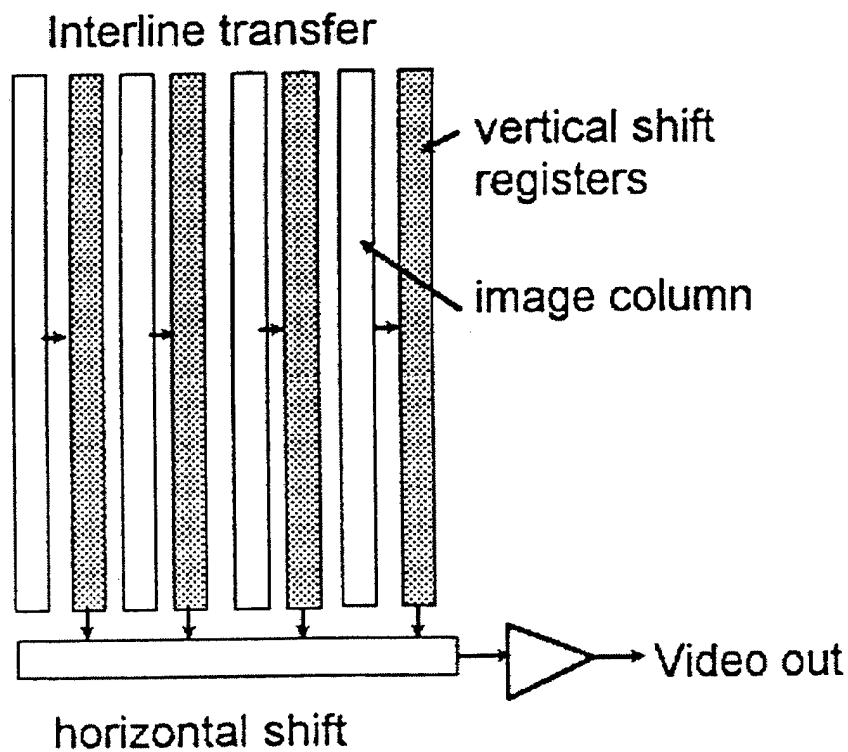


Figure 12: CCD Data Output Circuit. Taken From Walters, (1990).

the CCD chip. Unfortunately, the tapered fiber-optic bundle generated an intolerable amount of distortion for the AMI application due to its demagnification process.

Electro-optical Services Inc. located in Charlottesville, VA, was contracted to manufacture an optical coupler between the IIT and CCD. Now, the COTS requirement added to our challenge. MUSTANG's direct coupling between IIT and PCD made for a very compact detector assembly. Since the instrument was used in sounding rocket experiments, MUSTANG's designers were pretty stingy with its real estate (See **Figure 13**). As a result, there wasn't much clearance between the back of the off axis telescope and the detector assembly. Naturally, we desired the overall length of the DUUVIS detector assembly to remain consistent with that of MUSTANG in order to avoid having to build a new telescope. Unfortunately, the commercially available lenses under consideration for the new optical coupler possessed focal lengths which precluded matching detector assembly lengths and fabrication of lenses to meet that requirement were simply cost prohibitive. There were other considerations as well. Should the mapping of the IIT be fully contained in the detector or vice versa (i.e. should the circle be contained within the rectangle or the rectangle be contained within the circle)? At that time, the AMI experiment was in full swing so we decided on the "circle in a square" mapping to maximize the resolution of the fringes observed with the AMI. **Figure 14**

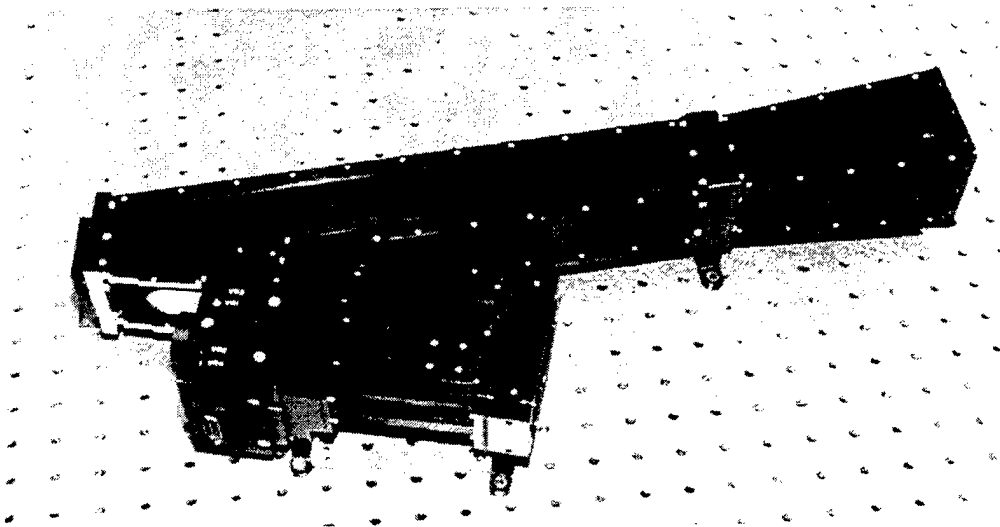


Figure 13: The MUSTANG Instrument: Telescope, Spectrograph, and Detector Assembly.

illustrates the geometry of the mapping¹. Once the mapping geometry was determined, the most challenging dimension became the length of the reduced radius section at the front end of the lens coupler assembly. The focal plane of the instrument was located 0.151" from the rear face of the spectrograph. There was only 0.564" clearance between the back of the grating and the rear face of the spectrograph. This implied the front of the lens coupler casing could not extend over 3/8 of an inch beyond the focal plane to allow for positioning of the grating. Ideally, the photocathode should have been positioned in the focal plane. In reality, the focal length (i.e. the distance from the outer surface of the entrance window to the S-20 coating) of the photocathode was 0.250" \pm 0.050". Assuming a 1/16" (0.0625" \pm 0.005") minimum thickness for the retaining lip on the front of the casing, the worst case scenario was that the front of the lens coupler casing would extend 0.519" beyond the focal plane. This would clear the back of the grating by 0.045" (less than 1/16 of an inch). **Figure 15** contains a block diagram of the lens

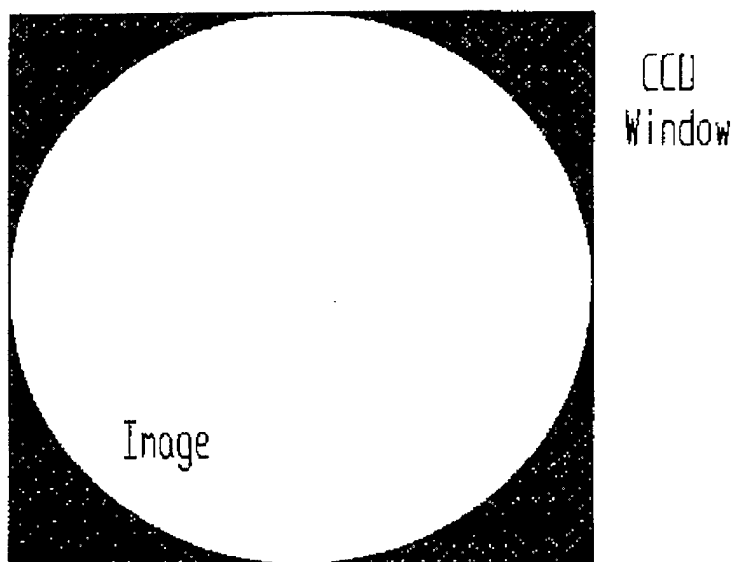


Figure 14: Coverage of CCD Input Window by the Image From the Lens Coupling Device. Taken from Hicks (1995).

¹ While this decision was optimal for AMI, it was less than optimal for DUUVIS.

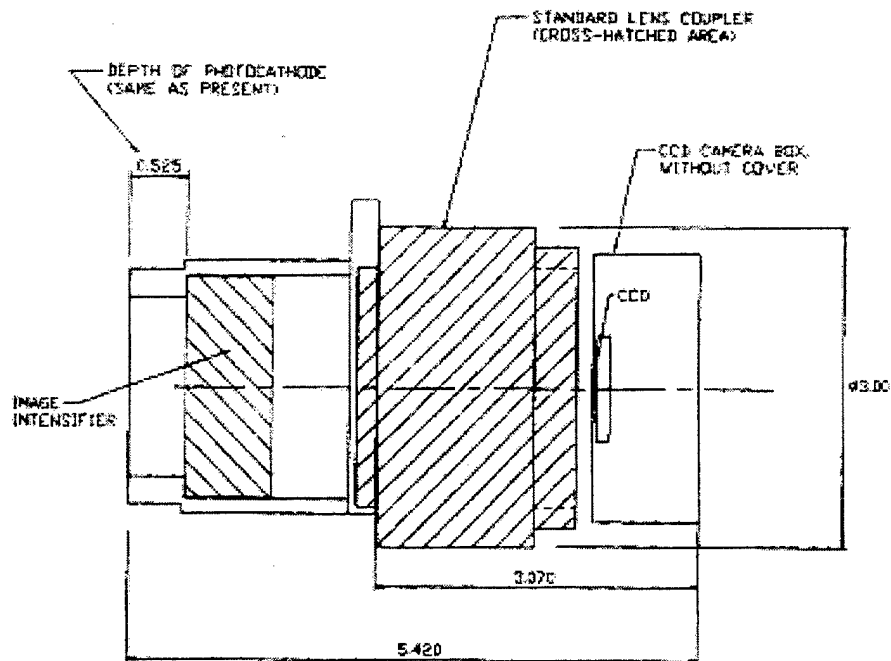


Figure 15: Block Diagram of the Lens Coupler Assembly.

coupler assembly. In spite of the close tolerances, and after numerous phone calls and facsimile exchanges, an acceptable detector assembly was delivered in November 1995.

Upon arrival of the new detector assembly, the next challenge was to mount it onto the spectrograph while preserving the integrity of the off-axis telescope. This was a rather delicate operation. A mounting clamp was designed consisting of two half shells which, when bolted together, provided support for the lens coupler in addition to providing a means for attaching it to the spectrograph. The clamp was manufactured by the Physics Department Machinist and subsequently, the painstaking process of fitting the lens coupler with the telescope began. The mounting clamp, located at the front of the DUUVIS detector assembly, is shown at the top of **Figure 16** which illustrates the size difference between the MUSTANG and DUUVIS detector assemblies. Both the telescope and lens coupler were made of aluminum with fairly thin wall thickness. If too much metal was removed from any given area, the section being reduced would begin to tear and the integrity of the component would be violated. An iterative cycle of disassembly, machining, reassembly, and measurement was implemented to ensure just

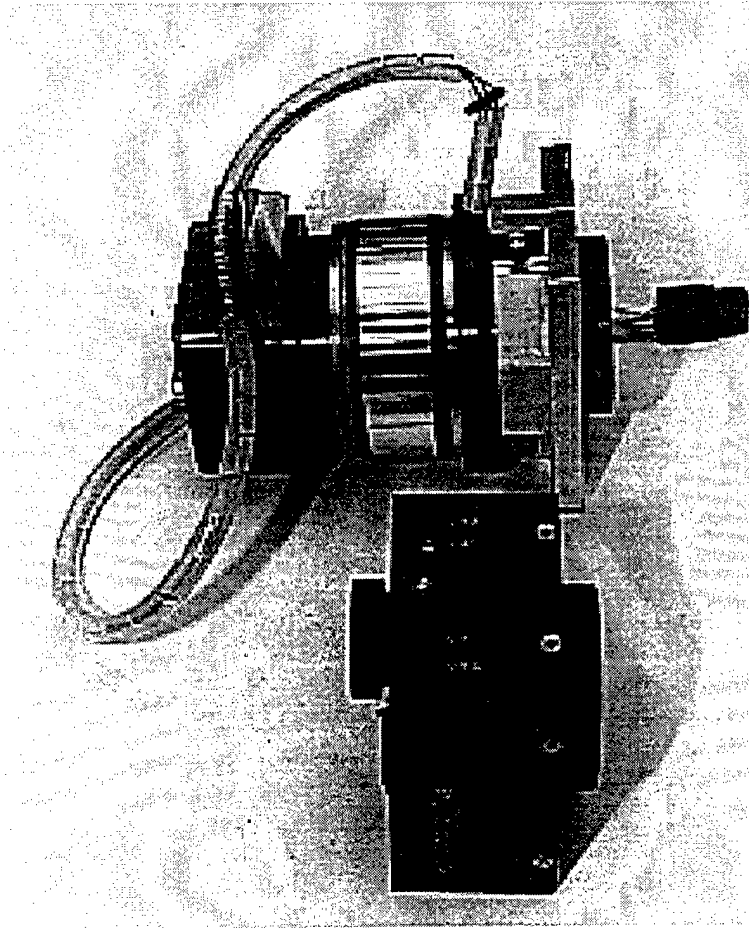


Figure 16: Comparison of DUUVIS and MUSTANG Detector Assemblies.

enough metal was removed from the right places. The result of this process was a very precise fit to a tolerance of 0.001". An appreciation of the close fit between the telescope and the DUUVIS detector assembly can be gained by viewing **Figure 17**. The shiny ring in the middle of the lens coupler was originally a knurled adjustment ring similar to those found on telephoto lenses. When the telescope could no longer be machined, the coupler was disassembled, the ring removed and machined. Putting a knurled finish on the ring subsequent to machining would require it to be clamped so tight in the chuck of the lathe that it might result in damage to the internal threads. The solution to this problem was to cut longitudinal grooves in the ring. They could be inserted without risking damage to the internal threads and still provide enough texture to grip onto while adjusting the focus of the lens coupler assembly.

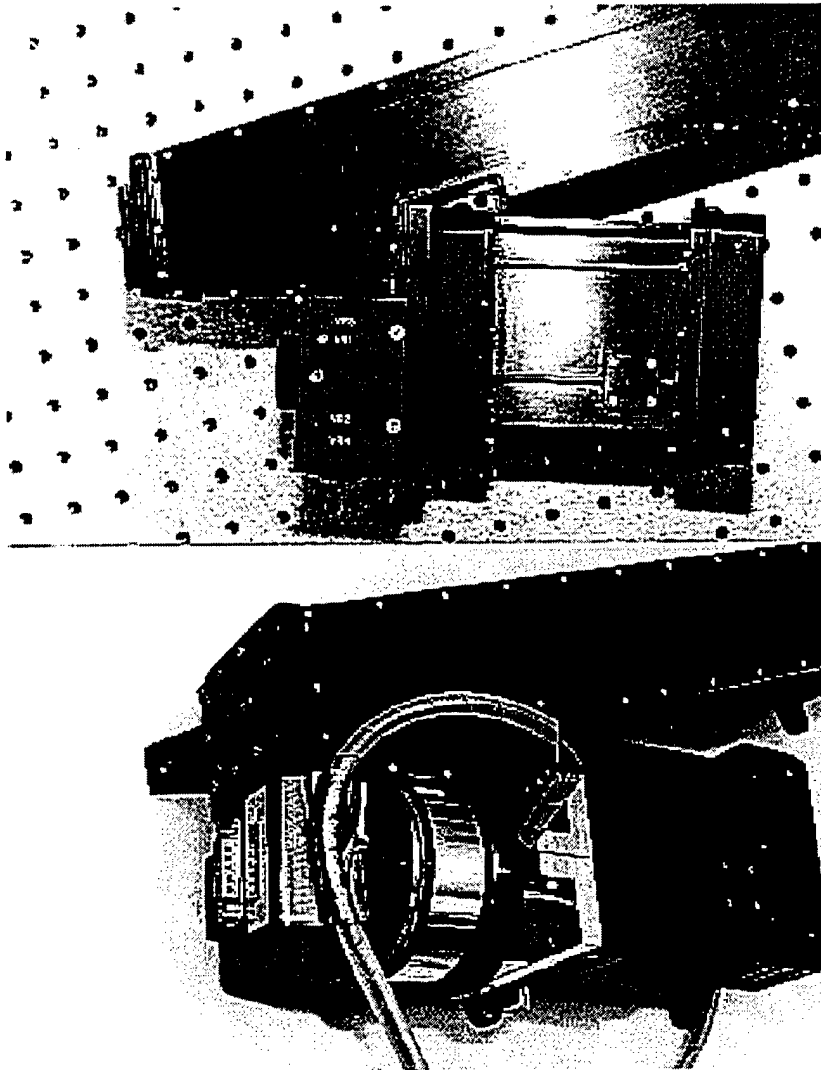


Figure 17: Comparison of Installed MUSTANG (top) and DUUVIS (bottom) Detector Assemblies.

C. SCANNING MIRROR INSTALLATION

Several possibilities were considered for control of the scanning mirror. Initially, a motor and cam assembly was envisioned for positioning the mirror, then the possibility of making the mirror shaft out of two-way shape memory NiTi alloy (sexy technology) was considered. Neither of these designs provided the accuracy required for this application. Due to the position accuracy requirement and potential need for high speed slewing, a servo-controlled mirror assembly was finally chosen. The M3 series optical scanner, a high speed galvanometer designed for advanced beam positioning, commercially available from General Scanning Inc. proved worthy of the task. The M3 scanner uses a "moving-magnet" design which enables it to move at high speed over wide angles (total range of $\pm 30^\circ$ of travel) with precise angular positioning. Additionally, the M3 maintains the low inertia rigidity and temperature control of moving iron devices while retaining the low inductance of a moving coil unit. General Scanning, located in Watertown, MA, was chosen based on their outstanding reputation for high quality scanning components and their twenty five plus years of experience in the field.

Again, financial limitations added to the challenge. Our budget did not allow purchase of the complete system with all necessary electronics contained in a Eurocard chassis. Instead, we purchased the M3 galvanometer, a MgF_2 coated (UV sensitive) "Y" mirror, an electronic digital driver (EDD) with backplane, and a six foot cable (for connecting the galvanometer to the backplane), with the understanding that we would have to furnish power to the EDD and provide the computer interface. Dimensions for the Y mirror and M3 galvanometer are provided in **Figure 18**. While awaiting arrival of the scanner components, computer interface requirements were identified. Control of the M3 scanner is accomplished by sending a 16 bit binary word from a personal computer (PC) to the EDD. The EDD then converts the digital input signal into an analogue output signal which repositions the galvanometer. General Scanning provided guidance on selection of a compatible digital input/output (I/O) card for the computer as well as some programming suggestions (written in C++) for galvanometer control.

Table 2. Example of PCDIO-48P Signal Transfer

MSB

1797 = 0 0 0 0 0 1 1 1 0 0 0 0 0 1 0 1

Port Address: B7 B0 A7 A0

LSB

PORT	PIN NUMBER	VOLTAGE (Vdc)
A	0	+ 5
A	1	0
A	2	+ 5
A	3	0
A	4	0
A	5	0
A	6	0
A	7	0
B	0	+ 5
B	1	+ 5
B	2	+ 5
B	3	0
B	4	0
B	5	0
B	6	0
B	7	0

Scanning requirements for DUUVIS are driven by two factors, the horizontal IFOV (1.12 mrad), and the exposure time required for the CCD to collect the image. The typical DUUVIS scan cycle would be to step the mirror 1 mrad, pause, save the image, and repeat through the desired horizontal FOV. A 16 bit binary word allows us to express integers ranging from 0 to 216 (65,536). This implies that the minimum increment of movement for a scanner with a 60° total arc of travel is 60/65,536 degrees or 16 μ rad. DUUVIS did not require 60° of rotation so our M3 galvanometer was tuned at the factory to set it's arc of travel to +/- 10°. Recalculation of the minimum increment of movement yields 20/65,536 degrees or 5.3 μ rad. Actual positioning of the mirror would be in one mrad increments which translates to 188 bit increments in the C program controlling mirror position.

Upon receipt of the scanning equipment, several additional components had to be fabricated. First, an adapter had to be designed to house the M3 scanner and allow for mating with both the telescope and the sun shade. The adapter was designed to position

the scanning mirror at a 45° angle to the optical centerline of the telescope. This would minimize the vignetting effect of the scanning mirror. The height of the galvanometer casing dictated that it should be mounted on top of the adapter. **Figure 19** shows the configuration of the scanning mirror adapter when fully assembled. Close inspection of **Figure 19** reveals a seam in the adapter at the base of the cylinder which houses the galvanometer barrel. The scanning mirror is wider than the diameter of the galvanometer barrel making it necessary to remove the top of the adapter to attach the scanning mirror to the galvanometer shaft. This is illustrated more clearly in **Figure 20**.

The next items needed to be fabricated were a chassis to mount the EDD and backplane, and ribbon cable to provide the connection between the 50 pin I/O connector on the PC-DIO48-P and the input to the EDD. The chassis, shown in **Figure 21**, was made in the student workshop out of excess material from discarded items. A standard 50 pin ribbon cable was modified to make the connections shown in **Table 3**.

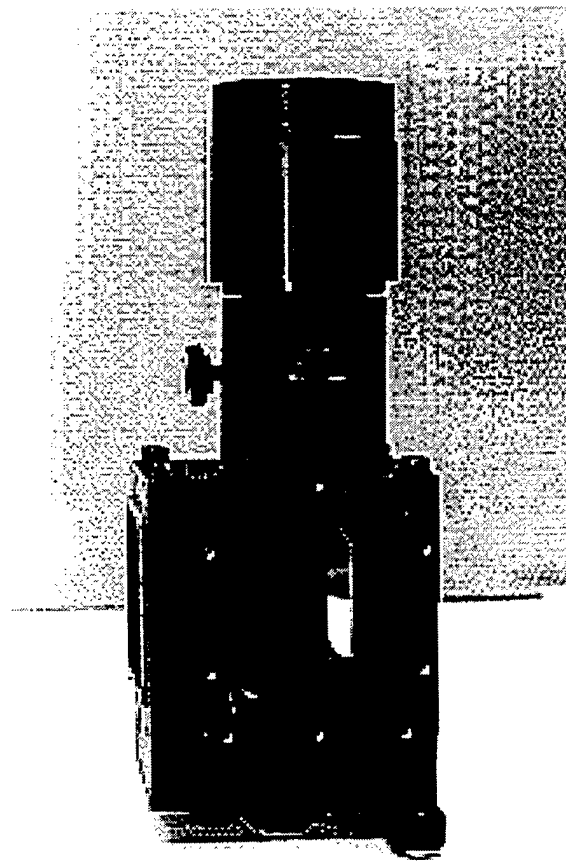


Figure 19: Scanning Mirror Adapter Completely Assembled.

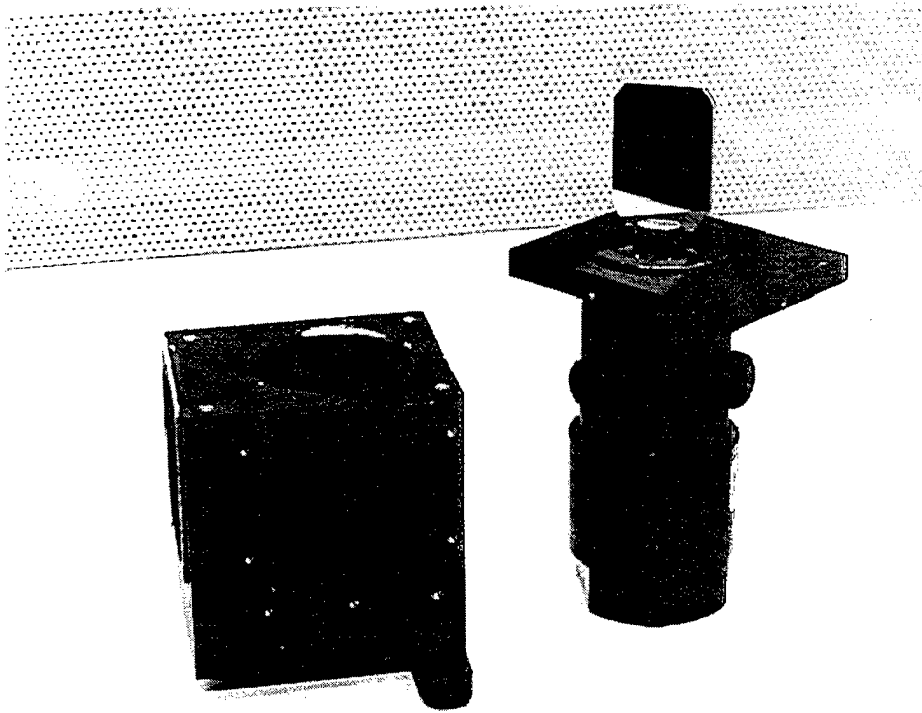


Figure 20: Scanning Mirror Adapter Partially Disassembled.

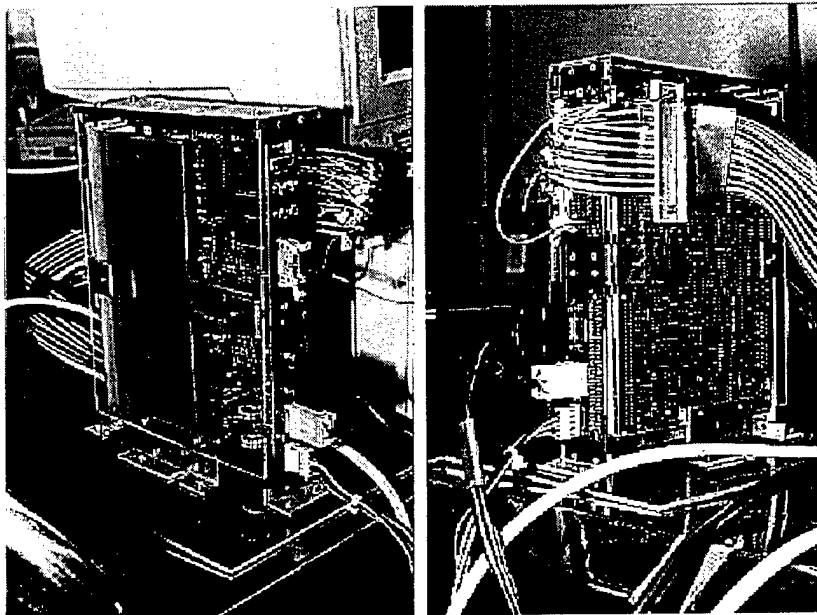


Figure 21: EDD Chassis with Backplane.

Table 3. PCIO 48 to EDD Wiring List

Signal Name	8255 Port Address	PCDIO48 P1 Pin #	Backplane J1 Pin #
D0	B0	31	A1
D1	B1	29	A2
D2	B2	27	A3
D3	B3	25	A4
D4	B4	23	A5
D5	B5	21	A6
D6	B6	19	A7
D7	B7	17	A8
D8	A0	47	C1
D9	A1	45	C2
D10	A2	43	C3
D11	A3	41	C4
D12	A4	39	C5
D13	A5	37	C6
D14	A6	35	C7
D15	A7	33	C8
A1	C0	15	C13
A2	C1	13	C14
A3	C2	11	C15
A4	C3	9	C16
RESET	C4	7	NOT USED
STROBE	C7	1	A10
RD/WR(DIR)	C5	5	A12
+ 5 Vdc	N/A	49	C32
GND	N/A	50	A32

Although the wiring requirements listed in **Table 3** seem pretty straight forward, accomplishment of the task proved to be non-trivial. J1 and J2 on the backplane are 96 pin connectors, configured as 3 columns of 32 rows, with the center column not used. The backplane only had a female connector for J2. No connector was provided for J1. The EDD plugs into the backplane so as to form a "T". This leaves approximately 1/4 inch of clearance between the male connector (P1) on the EDD and the backplane. There isn't enough room to plug in a 90° connector (if one were even available) into P1 and still clear the backplane. The M3 Scanner/Driver User Manual furnished by General Scanning does not contain a schematic of the EDD, nor does it outline a detailed procedure on how to connect the EDD to a digital I/O card. Initially, this caused considerable amount of

confusion as to the function of J1. Time was growing short and no 96 pin female connectors were locally available, so ingenuity was forced to take control. Pin extenders were made by soldering IC socket pins (See **Figure 22**) onto female connectors from a standard 25 pin "D" connector. The extenders were insulated with heat shrink tubing and slipped onto the appropriate pins of P1. Proper alignment of the EDD with the backplane to allow the 25 pin extenders to pass through the correct holes on the backplane required a significant amount of patience. Once the EDD was mated with the backplane the top of the chassis served to lock the pins in place. Female socket connectors were then soldered onto the appropriate leads on the ribbon cable. Each of the ribbon cable connectors was

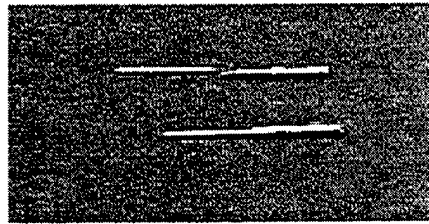


Figure 22: Pin Extenders for EDD Connector P1.

then insulated with heat shrink tubing, labeled, and attached to the appropriate pin of J1.

The last items to be acquired were power supplies. Power requirements for the M3 scanner are identified in **Table 4**.

Table 4. EDD Power Requirements

VOLTAGE	CURRENT
+ 18 Vdc	1.5 A @ continuous, 3 A peak
-18 Vdc	1.5 A @ continuous, 3 A peak
+ 5 Vdc	1.5 A Max.

Three Hewlett Packard power supplies, two HPE3615A's and one HP6216B, were obtained and a connector cable was fabricated to plug into J5 on the backplane. DUUVIS was completely assembled.

The final DUUVIS configuration is illustrated in **Figure 23**. The entire DUUVIS system including EDD, backplane, PC, power supplies, and associated cabling is shown in **Figure 24**. As mentioned previously, the closest thing to a schematic available in the M3 Scanner/Driver User Manual is illustrated **Figure 25**.

D. SOFTWARE DEVELOPMENT

With DUUVIS completely assembled, the only missing ingredient was the software to coordinate the operation of all its individual components. The amount of effort required to accomplish this task was by far the most underestimated aspect of the experiment. If DUUVIS is to operate on a UAV in future experiments, it must be able to function autonomously. This requires "hands-off" operation after initiation of a master program. As previously mentioned, all the individual DUUVIS components are advertised as being capable of operating in this manner. Unfortunately, there are many subtle barriers that are not readily apparent until the individual components begin to interact.

The principle of operation is simple enough. After the desired FOV has been determined, the main program slews the mirror over to one end and begins to step it through the FOV in 1 mrad increments. At each step, the detector is exposed to the incident radiation for the appropriate amount of time, after which it stores the image to disk as a TIFF file. The cycle repeats for each step through the entire FOV. In practice, this process would continue until the entire area of interest were imaged. For the sake of simplicity, this discussion will only address one sweep through the entire FOV. In an attempt to minimize start up time for the instrument, this effort pushed the development of a program in C++ for instrument control. This was the *easiest* path to compatibility with the equipment manufactures since most PC application software is written in C. Saving the files in TIFF format for subsequent compilation into a multi-dimensional array for data analysis is a cumbersome method of operation. That bridge will have to be crossed at a later time. The numerous bugs which surfaced during this experiment precluded software development beyond successful control of the instrument. The actual program "MSCNSCAN.C", is provided in the Appendix. A general overview of the

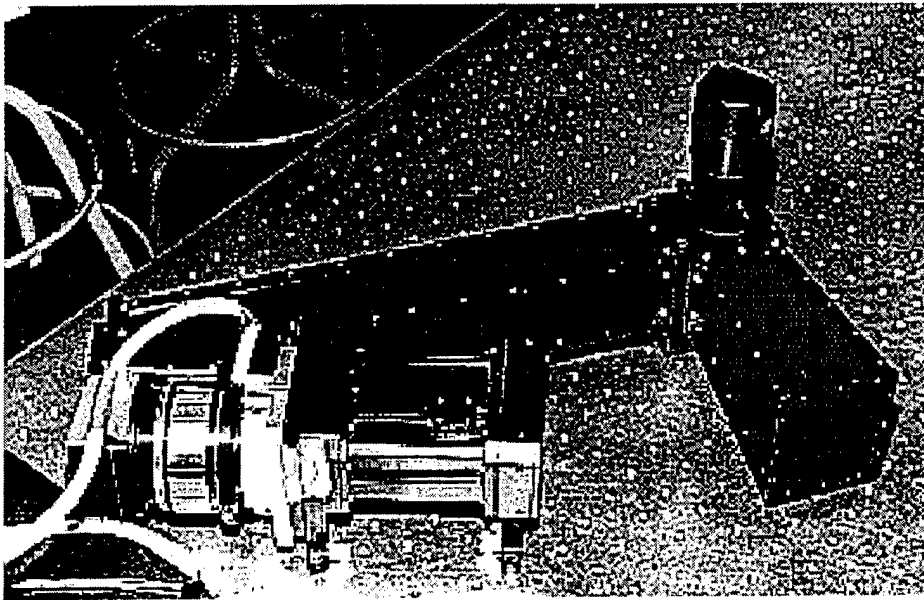


Figure 23: Final DUUVIS Configuration.

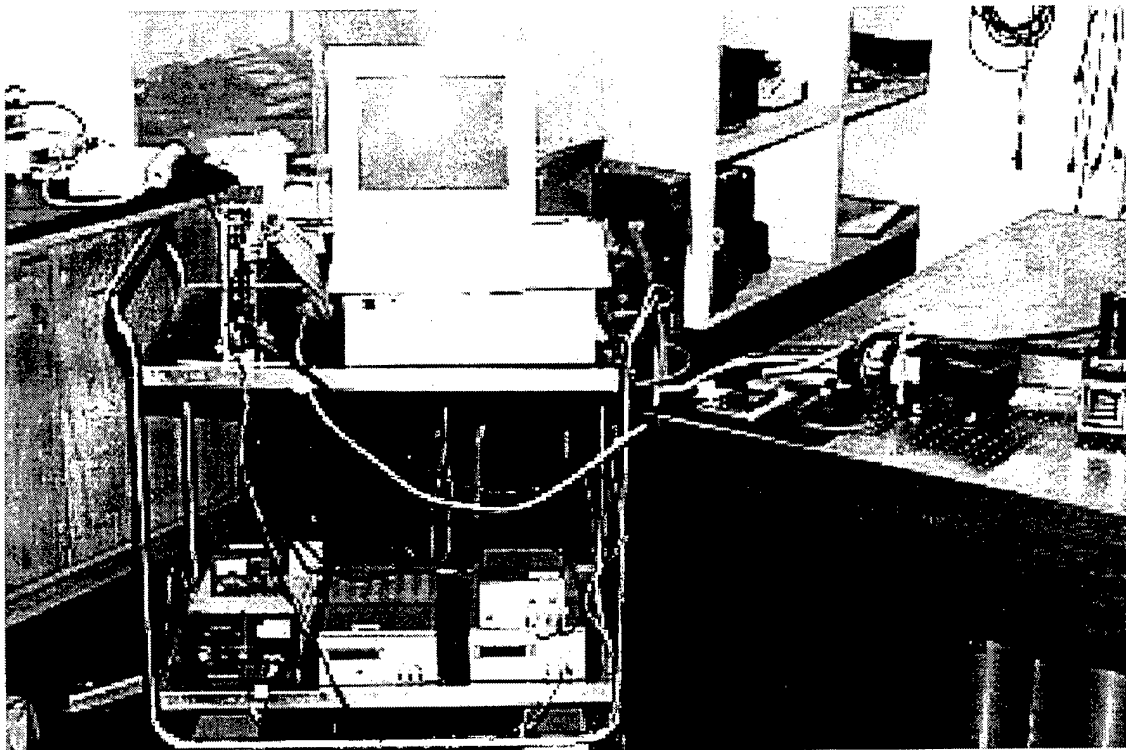


Figure 24: DUUVIS with Associated Support Equipment.

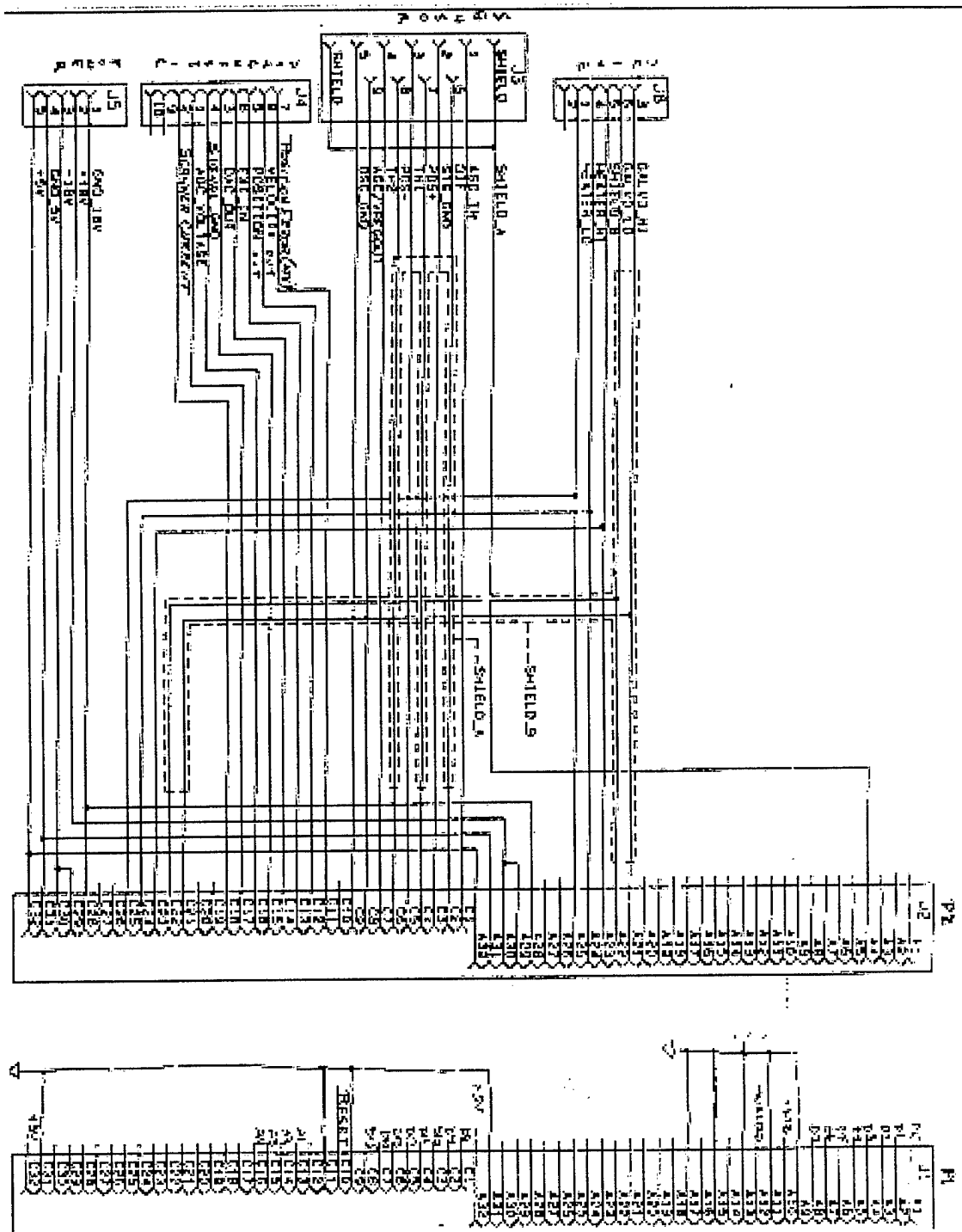


Figure 25: EDD Backplane Wiring Schematic. Taken from General Scanning (1992)

program and some of the problems encountered during its development are discussed herein.

There are three primary components which must successfully interact for DUUVIS to function, namely, the digital I/O card, the M3 scanner, and the digital camera. Program development was aimed at conquering each component individually prior to incorporating them into the main program.

The first component addressed was the digital I/O card. As mentioned in the previous section, control of the mirror is accomplished by passing a 16 bit binary word to the PCDIO48 which, in turn, delivers a digital signal to the EDD card. In decimal values, 0 represents the limit of travel in one direction ($+ 10^\circ$), 32,768 represents the center of travel (0°), and 65,536 represents the limit of travel in the opposite direction ($- 10^\circ$). Operation of the PCDIO48 in Mode 0 is pretty simple. The base address of the I/O card is 300 hex. Addition of a 0, 1, or 2 to the base address provides access to Port A, B, or C respectively. To set the mode on the 8255, add a 3 to the base address and send an 80 hex. This sets only the MSB of the control register of the 8255 HIGH with all other bits LOW which configures the 8255 for mode 0 operation with all output ports. Every word passed to the PCDIO48 from the program automatically results in a corresponding digital signal being sent to the backplane through the ribbon cable.

Once the digital signal is present at J1 of the backplane, the EDD must be directed to read it and convert it to a position command. This direction is achieved by toggling the strobe. Refer to the timing diagram in **Figure 26**. STROBE is a leading edge triggered control signal. At program start, RD/WR is set LOW (WRITE) and remains at that value for the rest of the program. Strobe (Port C, pin 7) is set LOW before a new digital signal is sent over D0 through D15 (Port B and Port A respectively, all pins). When STROBE goes HIGH again, the EDD reads in the new digital signal on D0 through D15 and converts it into a new position command.

Now the program is able to control the position of the scanning mirror. At each position, it must obtain an image and subsequently store it to disk. This is where the real problems arise. Electrim Corporation furnishes several programs to facilitate the use of their cameras. However, they keep the source code for manipulation of the CCD itself

Description	Symbol	Min.	Typ.	Max.	Units
Control Setup	TCVSL	10	-	-	nS
Data Setup	TDVSH	20	-	-	nS
Strobe	TSLSH	100	-	-	nS
Control Hold	TSHCX	20	-	-	nS
Data Hold	TSHDX	100	-	-	nS
DAC cycle	TSHCC	-	8	-	μ S

NOTE: Address Setup & Hold times are identical to those of Control lines.

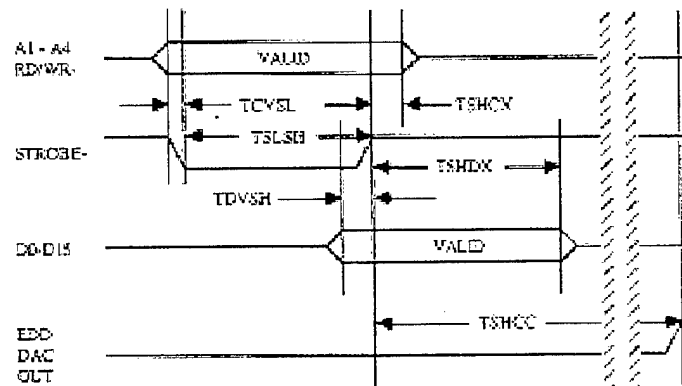


Figure 26: Bus Write Cycle Diagram. Taken from General Scanning (1992).

proprietary. They do provide "Linkable Routines" which allow for slight modification of their programs to perform a variety of functions including saving images to disk in TIFF format. The functions called out by the linkable routines are contained in various object files (furnished by Electrim) which have already been compiled in Microsoft C 8.0. The source code for control of the scanner was written in Borland C++. That version of C was chosen because it contains the *outportb* command which was referenced in General Scanning's sample program for scanner control. After many painful hours of self study in compiling and linking, the incompatibility of Borland C++ and Microsoft C became an insurmountable obstacle. There was no way to determine Electrim's function protocols, and the linkable routine for writing TIFF files would never suffice as written, since it utilized only one file name as it was designed to terminate upon successful image storage. After successfully writing a routine for generating sequential filenames, a copy of Microsoft Visual C++ Ver. 1.52c. was obtained to be compatible with the Electrim object files. One minor problem, Visual C++ doesn't contain the *outportb* command so the *_outp* command had to be used for sending binary words to the digital I/O card.

"MSCNSCAN.C", listed in the Appendix, is the program which finally proved successful in stepping the scanning mirror through a scene while collecting an image file at each position increment along the way. Results obtained with this program are provided in the following chapter.

IV. DATA COLLECTION

Two UV source lamps were used to conduct initial testing of DUUVIS, a mercury (Hg) lamp with 5 spectral emission lines, the strongest of which is at 254 nm, and a platinum (Pt) hollow cathode lamp with 23 spectral emissions between 180 nm and 340 nm [Hymas, 1994]. A wavelength calibration has not yet been conducted on DUUVIS, thus the exact correlation between pixel and wavelength is unknown. However, the images contained herein do illustrate the two-dimensional property of the DUUVIS detector in addition to exploiting some of the spectral features of the source lamps themselves. This is illustrated in **Figure 27**, a static image taken with the 1200 l/mm grating installed in the instrument. In this image, the two source lamps are separated in height. The spectra along the bottom of the image is that of the Pt lamp. Comparison of the spectral features contained in the image to those of **Figure 28** show a nice correlation of the Pt spectra leading us to believe the bandpass is fairly close to the estimated value of 195 nm to 330 nm. Also, the bright line above the Pt spectra, appears to be the strong Hg emission at 254 nm. **Figure 29** is an image of the same scene with

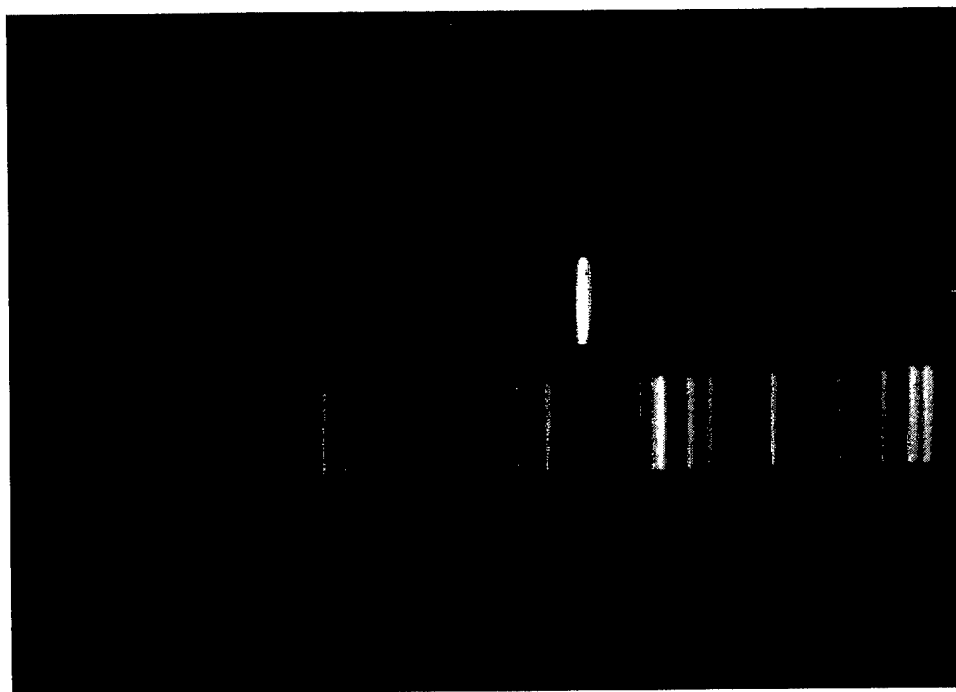


Figure 27: DUUVIS "Snapshot" of Pt and Hg Lamp Spectra taken on 02 DEC 96.

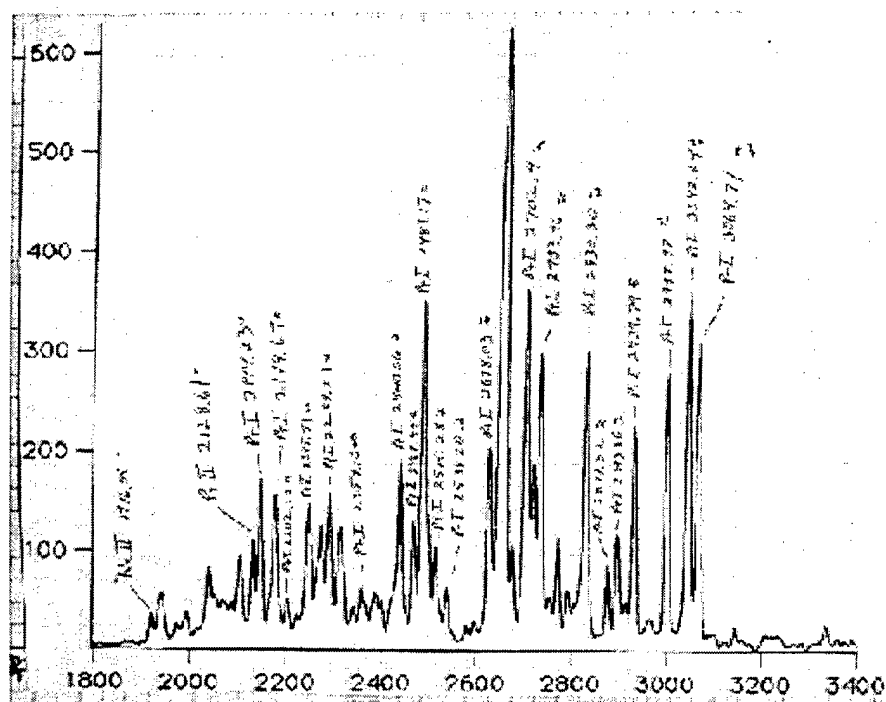


Figure 28: Platinum Hollow Cathode Lamp Spectra. Taken from Cleary (1996).

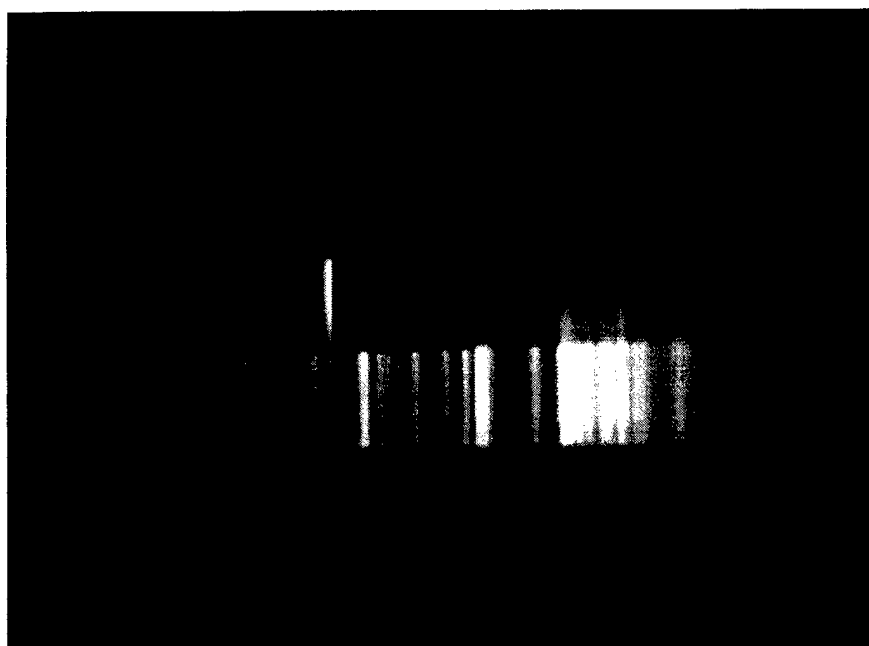


Figure 29: DUUVIS "Snapshot" of Pt and Hg Lamp Spectra taken on 04 DEC 96.

the 600 l/mm grating installed. In the left two thirds of the image we observe a similar pattern to that of **Figure 27**. The bright lines in the right one third of the image are believed to be in the visible portion of the spectrum. If this is true, then we are observing a spectral bandpass which is approximately between 190 nm and 480 nm. So far, the images presented in this section have been static. As previously mentioned, software problems curtailed progress in the area of data analysis. As a result, there is no hyperspectral cube to display. A feel for the dynamic properties of DUUVIS may be gained through **Figure 30 a thru o**. To actually scan through a 2.5° FOV would require 88 "snapshots". In **Figure 30**, 15 consecutive snapshots are presented thus illustrating the scanning capability of the instrument. For this image, a slight separation distance was introduced between the source lamps in both the horizontal and vertical directions. As DUUVIS scans through a 0.9° FOV (moving from left to right and top to bottom on the page) we observe a very strong Hg signature in the first few frames. The Hg begins to fade out around frame "g" and is completely gone by frame "i". In similar fashion, the Pt signature continues to grow stronger until it peaks out in frame "o".

All the images presented thus far have been in the form of vertical spectral lines. Although this is quite normal in spectroscopy, it is not very desirable for imaging applications. A simple test to obtain a feel for the instrument's point spread function (PSF) was conducted by positioning the Hg lamp approximately two meters away from the entrance of DUUVIS' sun shade. A shroud was placed over the lamp and two pin holes were poked through it. Initially, we observed no difference, that is, we still observed a vertical spectral line even from a point source. After some consideration, we realized this is a property of an "off-axis" optical instrument. When an object lies an appreciable distance off of the optical axis (as is the case in the DUUVIS spectrograph), the incident cone of rays originating from that object strike the lens asymmetrically. This causes an aberration known as astigmatism. See **Figure 31**. In an off-axis instrument, there are two distinct focal lengths which cause the cone of rays to become elliptical. The focal plane of our instrument is the tangential focal plane (represented by F_T in the illustration) in which the ellipse degenerates into a line. This explains why our simulated

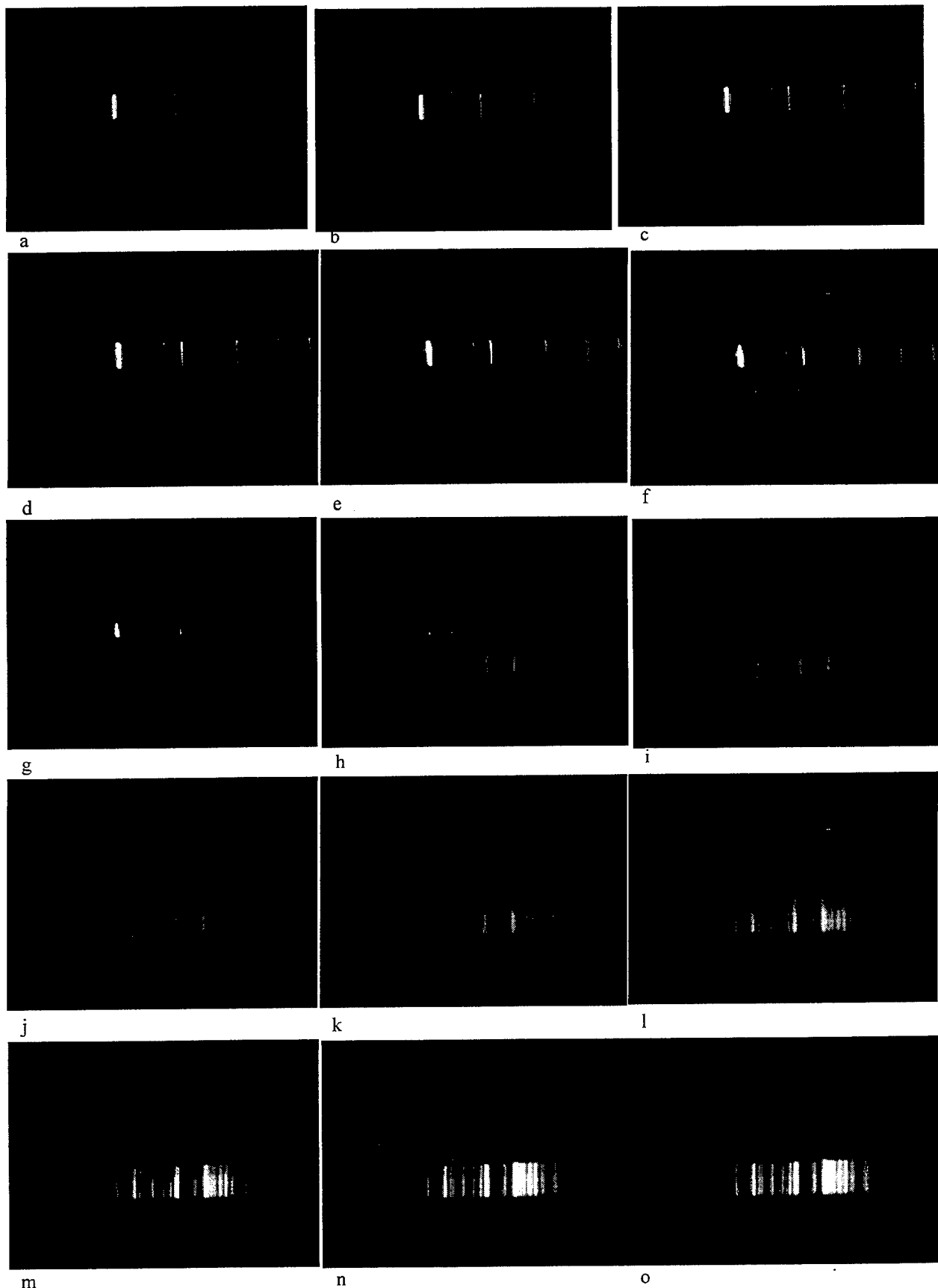


Figure 30: Pt and Hg Lamp Spectra Obtained During DUUVIS Scan of 0.9° FOV taken on 08 DEC 96.

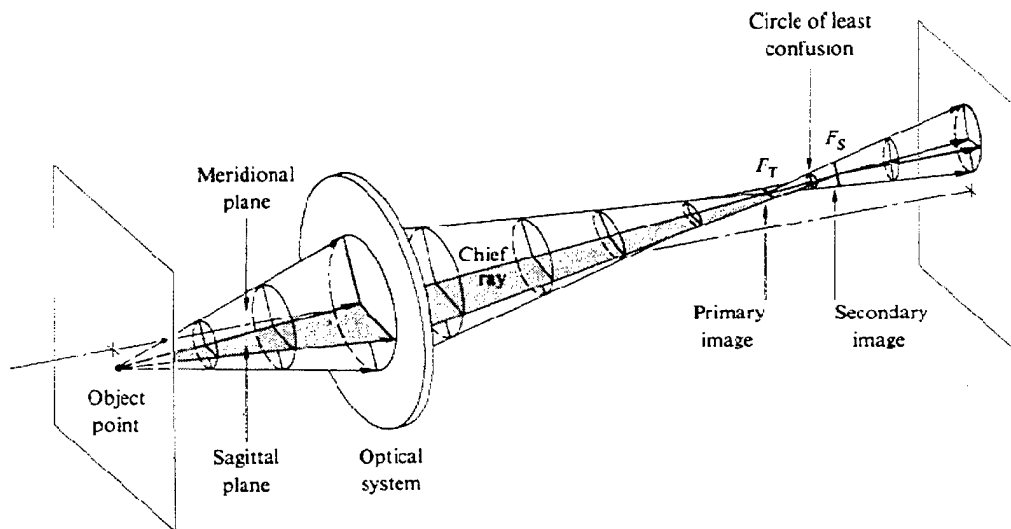
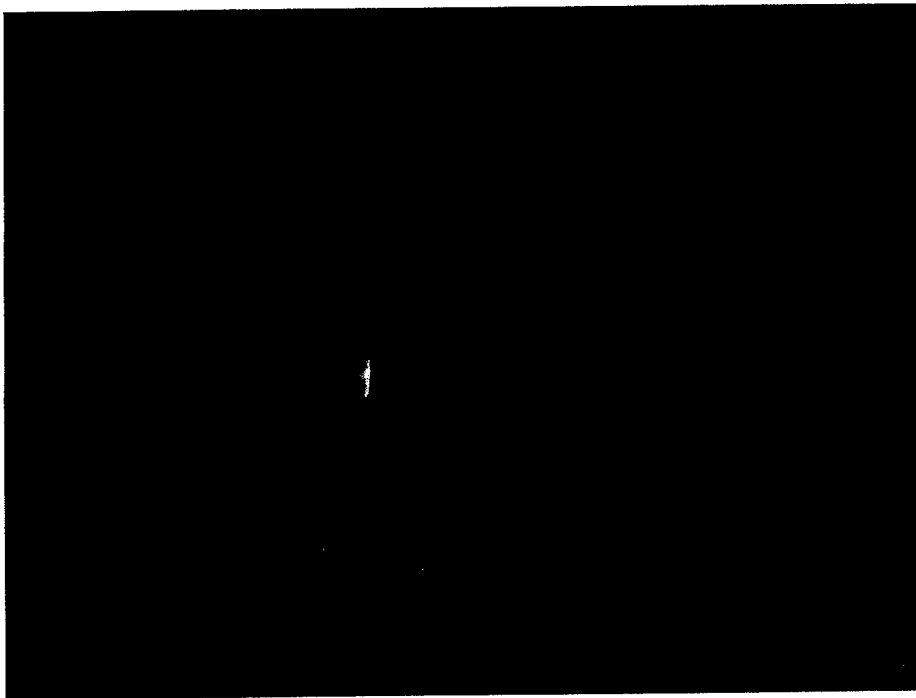


Figure 31: Illustration of Astigmatism. Taken from Hecht (1987).

point source appeared as a line on the detector. Again, this is good for spectroscopy but doesn't lend itself to imaging.

Seeking improved performance, the mounting clamp for the lens coupler assembly was loosened and the entire assembly was moved back (away from the spectrograph) in an attempt to move the photocathode behind the tangential focal plane. The result of this adjustment is shown in **Figure 32**. The point spread function was clearly reduced but further adjustment is necessary.



**Figure 32: DUUVIS "Snapshot" of a Simulated Hg Point Source taken on
09 DEC 96.**

V. CONCLUSION

A. SUMMARY OF FINDINGS

The main objective of the research described in this thesis was to design, fabricate, and test the first MUV hyperspectral imager. Design began with the NPS MUSTANG instrument. MUSTANG's one-dimensional detector was replaced with a two-dimensional image intensified CCD. The new two-dimensional detector required an optical coupler to map the image from a circular aperture IIT down onto a rectangular detector area. As a result of the optical coupler, the new detector assembly was twice the length of its predecessor. Great care was taken in mounting the new detector assembly to preserve the integrity of the existing off-axis telescope. A servo-controlled scanning mirror was then mounted to the front of the telescope. Budget constraints required design and fabrication of a chassis to house the control circuitry for the scanning motor in addition to design and fabrication of special cabling to connect the EDD to the digital I/O card. Three power supplies were acquired to provide the proper voltages to the EDD. A program for control of the instrument was written and compiled in Microsoft Visual C++. The first successful operation of DUUVIS occurred on 08 DEC 96. Unforeseen compatibility problems between Borland C++ and Microsoft C 8.0 resulted in schedule delays which precluded extensive testing of the instrument. The only data obtained by DUUVIS to date is spectra from two calibrated UV source lamps.

B. RECOMMENDATION FOR FURTHER RESEARCH

There are two categories of software development associated with this effort; software for control of the instrument, and software to enable analysis of the data after it has been collected. Numerous problems encountered during the development of the initial instrument control software, precluded any progress toward data analysis. In this experiment, it was necessary for instrument-control software to be developed first in order to obtain a working instrument. Approaching the problem from the opposite end might prove to be more productive. The premiere software on the market for analysis of

hyperspectral imagery is ENVI. It is a very powerful software package that is written in the Interactive Data Language (IDL). IDL has the capability to control peripheral devices. The instrument would operate much more efficiently if it could continuously download data to an ENVI file vice store each snapshot as a TIFF and subsequently combine files to make an image. There is potential for very productive research in this area.

Before it can provide useful data, the instrument must undergo a wavelength calibration. Additionally, the scanning mirror must be bore sighted to precisely determine it's FOV at the center position.

Finally, sensitivity tests should be performed on the instrument prior to it's first UAV flight. These three items could easily work into a thesis.

This initial cut at building a hyperspectral instrument was conducted on a shoestring budget. There are several aspects of the design which were accepted mostly because there was no other alternative. An example of this is the mapping of the intensifier image down onto the detector. Another example is the scanning mirror selection. Ideally, a larger mirror is desirable to eliminate vignetting. The mirror currently installed in the instrument was one of only two mirror sizes which the manufacturer offered with a (UV sensitive) MgF_2 coating. A trade off analysis should be conducted to determine how much improvement could be gained by upgrading the current design and at what point does it become advantageous to design a new instrument from the ground up based on lessons learned from DUUVIS. At the very least, a compact power supply needs to be manufactured for the instrument to replace the bulky laboratory type power supplies currently in use prior to DUUVIS's first UAV flight.

Finally, now that we have an instrument which extends the spectral range of the hyperspectral imagers currently in operation, there should be a schedule for frequent data collection. In the grand scheme of things DUUVIS is working it's way towards a volcanic ash cloud. There are many opportunities right here in our own back yard that shouldn't be overlooked, such as rocket plume spectra over at the NPS rocket engine test

facility. A trip to the beach might prove interesting to see how well DUUVIS performs in the 400 nm to 500 nm portion of the visible spectrum. Even in the lab, more tests should be conducted to determine the optimum positioning of the photocathode to minimize aberrations associated with off-axis optics.

APPENDIX


```

/* Erik O. Johnson */
/* 11 DEC 96 */
/* Program Name: MSCNSCAN.C */

```

```

/*****
/*
/*This program controls the operation of DUUVIS through one complete
/* scan through it's FOV. It contains commands obtained from the
/* htfsamp.c program provided by Electrim Corp. to save images to disk
/* in TIFF format. It also contains the basic I/O functions required by
/* the Electronics Digital Driver (EDD) to control the galvanometer for
/* DUUVIS' scanning mirror. It is based upon the sample code listed on
/* pages 44 thru 48 of the M3 Scanner/Driver Users Manual by General
/* Scanning Inc. Detailed descriptions of the functions called out in
/* this program are contained in the M3 Scanner/Driver Users Manual and
/* in the source code for htfsamp.c. This program was compiled in
/* Microsoft Visual C++ Ver. 1.52.
/*
*****/

```

```

/* SCENE SCAN FOR MICROSOFT VISUAL C++ */

```

```

#include <stdio.h>
#include <stdlib.h>
#include <conio.h>
#include <dos.h>
#include <malloc.h>
#include <math.h>
#include <string.h>

```

```

#define BASE1 0x300          // Base address of IO board for
#define DEV 0x000           // scanning mirror interface

```

```

#define A 0x0
#define B 0x1
#define C 0x2
#define P 0x3

```

```

#define BASE      (0x360)    // Base address of camera
                          // must match camera address

```

```

#define V      (244)        // Lines per field
#define H      (753)        // Bytes returned per line

```

```

#define KEYBOARD_CHECK (!0)
#define DEFAULT_EXPOSURE (100L) // 100 millisecond exposure

#define BiasValue (127) // mid scale of bias range
#define GainValue (175) // 2/3 scale of gain range

typedef unsigned char pixel; // one byte per pixel
typedef pixel __far * __far *field; // field is a pointer to an
// array of pointers

// Linkable Routines Function Prototypes:
unsigned short int __cdecl __far
highcam1 (unsigned int, int, int, int, int, unsigned long int, field, int);

int __cdecl __far
init800 (void); // init vga to 800 x 600

void __cdecl __far
display_image (field, unsigned int, unsigned int);

void __cdecl __far
InitDAC (unsigned int); // initialize D/A converter

void __cdecl __far
SetBiasValue (unsigned int, unsigned int); // set bias D/A converter

void __cdecl __far
SetGainValue (unsigned int, unsigned int); // set gain D/A converter

unsigned short int __cdecl __far
write_TIFF(char *, unsigned int, unsigned int, field, unsigned int, unsigned int,
           unsigned int, unsigned int); //save image as a tiff file

void __cdecl __far
set_ch_mode(); // set VGA to character mode

// HIGHCAM1 argument definitions:

unsigned int base = BASE; // base address of camera

```

```

unsigned long                                     // exposure time value in milliseconds
exposure_time = DEFAULT_EXPOSURE;               // for EDC-1000HR exposure control
pixel __far* buffer[V];                         // image buffer

// DISPLAY_IMAGE argument definition:
// Each line is displayed to the screen twice to give 488 lines total.
// Define storage for display buffer line pointers:

pixel __far* display_buffer[V*2];               // display buffer pointers

// Define the passing parameters

unsigned int AspcrXN, AspcrXD, AspcrYN, AspcrYD; // numbers for aspect ratio

unsigned int FV, FH;                            // height & width of the tiff image


void _cdecl
main(void)
{
    void startup(int);
    void shutdown(int);
    void galvo_send(unsigned int);
    void clrscr();

    char image_name[12], *duvis, *str1, *str2 = ".tif", *fname;
    double eoj_counter;
    int dec, sign, keyboard_check, ndig = 0;
    unsigned int MINPOS, MAXPOS, ILength, IWidth, position, retCode;
    int ctrlport, i, j, refresh_flag, ab_flag, interlace_flag, field_flag;
    long counter;

//    MINPOS=31452.0;
//    MAXPOS= 34460.0;
    MINPOS=24576.0;
    MAXPOS= 40960.0;
    eoj_counter = 100.0;
    position=32767.0;
    ctrlport=(BASE1+(DEV<<2)+P);
    startup(ctrlport);

```



```

for(position=32767.0; position>MINPOS; position=position-188.0)
{
    galvo_send(position);
    for(counter=1.0; counter<50.0; counter++)
        {}
}

for(position=MINPOS; position<MAXPOS; position=position+188.0)
{
    galvo_send(position);
//
    Flags:
        refresh_flag = !0;    // 0 disables RAM refresh
        ab_flag = !0;         // 0 disables anti-blooming
        interlace_flag = 0;    // !0 for interlace mode
        field_flag = 0;        // if interlace mode,
                                // 0 for first frame,
                                // !0 for second frame

//
    the return code is for checking the status of saving the file
    retCode=99;                // initialize the return code
    keyboard_check = !KEYBOARD_CHECK;
    ILength = V*2;             // number of lines to display
    IWidth = H;                // number of pixels to display
    duvis = "duvis";
    eoj_counter++;
    str1 = _fcvt(eoj_counter, ndig, &dec, &sign);
    strcpy(image_name, duvis);
    strcat(image_name, str1);
    strcat(image_name, str2);
    InitDAC (base);            // call only once at start
    SetBiasValue (base, BiasValue); // call to set bias voltage
    SetGainValue (base, 255 - GainValue); // call to set gain voltage
    // Allocate the image buffers:

    for (i=0; i<V; i++) {
        if ((buffer[i] =
            (pixel __far *) calloc ((size_t) H, sizeof (pixel)))
            == (pixel __far *) NULL) {
            cprintf ("\n\n\rCannot allocate memory for buffer!\n\r");
            exit ((char) -1);
        }
    }

    // Build display buffers from image buffers:
    for (i=0, j=0; i<V; i++, j+=2) {
        display_buffer[j] = display_buffer[j+1] = buffer[i];
    }
}

```

```

if (init800()) {      // init 800 x 600 by 256 color VESA mode 103
    cprintf ("\r\nVESA mode 103 not supported by display adapter!\r\n");
    exit (1);  }

    // Read the camera and display image:

for (i=0; i<4; i = ++i % V) {

    // Read the camera (ignore keyboard interrupt):

    highcam1 (base, refresh_flag, ab_flag, interlace_flag, field_flag,
        exposure_time, buffer, keyboard_check);
    display_image (display_buffer, ILength, IWidth);  }

    // Set the VGA to character/text mode

    set_ch_mode();

    // Save the last image as a TIFF file
    // Assign values to the parameters of write_TIFF before passing
    FV=244;
    FH=753;
    AspcrXN=753;
    AspcrXD=4;
    AspcrYN=244;
    AspcrYD=3;

//      buffer is already defined, buffer will be loaded by highcam1 procedure
//                                     // for write_big_TIFF proc
    fname=image_name;                // filename. tif extension
//                                     // in the filename is necessary.

    retCode=write_TIFF(fname, FV, FH, buffer, AspcrXN, AspcrXD,
        AspcrYN, AspcrYD);

//      print the return code

    cprintf ("\r\nThe return code is %d \r\n", retCode);

    for (i=0; i<V; i++) {
        free(buffer[i]); }
}

```

```

    for(position=MAXPOS; position>32766.0; position=position-188.0)
    {
        galvo_send(position);
        for(counter=1.0; counter<50.0; counter++)
            {}
    }

    shutdown(ctrlport);
    return;
} /* end of main */

void startup(int ctrlport)
{
    int mode0_out, cport, x_write;
    mode0_out=0x80;
    _outp(ctrlport, mode0_out);
    cport=(BASE1+(DEV<<2)+C);
    x_write=0x0a;
    _outp(cport, x_write); /* set RD/WR to write (LOW) */
    _outp(cport, (x_write | 0x80)); /* set strobe inactive (HIGH) */
    return;
} /* end of startup */

void shutdown(int ctrlport)
{
    int mode0_in;
    mode0_in=0x9b;
    _outp(ctrlport, mode0_in);
    return;
} /* end of shutdown */

void galvo_send(unsigned int position)
{
    int aport, bport, cport, x_write;
    aport=(BASE1+(DEV<<2)+A);
    bport=(BASE1+(DEV<<2)+B);
    cport=(BASE1+(DEV<<2)+C);
    x_write=0x0a;
    _outp(cport, (x_write & 0x7f)); /* set strobe active (LOW) */
    _outp(bport, (position & 0xff)); /* send LS Byte */
    _outp(aport, ((position & 0xff00)>>8)); /* send MS Byte */
    _outp(cport, (x_write | 0x80)); /* set strobe inactive (HIGH) */
    return;
} /* end of galvo_send */

```

LIST OF REFERENCES

- Atkinson, J. D. IV, "Implementation and use of a computational ray-tracing program for the design and analysis of complex optical systems", Master's Thesis, Naval Postgraduate School, Monterey, California, (1993).
- Cleary, D. D., Private Conversation, (1996).
- Cleary, D. D., S. Gnanalingam, R. P. McCoy, K. F. Dymond and F. G. Eparvier, "The middle ultraviolet dayglow spectrum," J. Geophys. Res., **100**, 9729-9739, (1995).
- Electrim Corp., EDC-1000HR Computer Camera Technical Manual, (1992).
- General Scanning Inc., M3 Scanner/Driver User Manual , (1992).
- Hamamatsu Photonics, Characteristics and Applications of Microchannel Plates, (1985).
- Hecht, Eugene, Optics, 2nd ed., Addison-Wesley Publishing Co., Menlo Park, CA, (1987).
- Hicks, J. D., "Design, development, and testing of the All-reflection Michelson Interferometer (AMI) for use in the mid-ultraviolet region", Master's Thesis, Naval Postgraduate School, Monterey, California, (1995).
- Holst, G. C., Electro-Optical Imaging System Performance, SPIE Press and JCD Publishing, Winter Park, FL, (1995).
- Hymas, H. M., "A calibration of the Naval Postgraduate School middle ultraviolet spectrograph and a analysis of the OII 2470 C emission obtained by the middle ultraviolet spectrograph", Master's Thesis, Naval Postgraduate School, Monterey, California, (1994).
- Industrial Computer Source, Model PCDIO Series Product Manual, (1995).
- Jet Propulsion Laboratory, "AVIRIS in a nutshell", <ftp://ophelia.jpl.nasa.gov/>, (1996).
- Klein, M. V., T. E. Furtak, Optics, 2nd ed., John Wiley & Sons, New York, (1986).
- Krueger, A. J., L. S. Walter, P. K. Bhartia, C. C. Schnetzler, N. A. Krotkov, I. Sprod, and G. J. S. Bluth, "Volcanic Sulfur dioxide measurements from the total ozone mapping spectrometer instruments", J. Geophys. Res., **100**, 14057-14076, (1995).
- Milton Roy Company, Diffraction Grating Handbook, 2nd ed., (1994).

Mobley, C. D., Light and Water, Radiative Transfer in Natural Waters, Academic Press Inc., New York, (1994).

Nordic Volcanological Institute, "NORDVULK Home Page", <http://www.norvol.hi.is/>, (1996).

Pearse, R. W. B., A. G. Gaydon, The Identification of Molecular Spectra, 3rd ed., John Wiley & Sons, New York, (1963).

Richards, J. A., Remote Sensing Digital Image Analysis, An Introduction, 2nd ed., Springer-Verlag, New York, (1993).

Samson, J. A. R., Techniques of Vacuum Ultraviolet Spectroscopy, John Wiley & Sons, New York, (1967).

Walters, D. L., PH4050 Class Notes, (1990).

Wilson, J., J. F. B. Hawkes, Optoelectronics, An Introduction, 2nd ed., Prentice Hall, New York, (1989).

Wolfe, W. L., G. J. Zissis, The Infrared Handbook, Office of Naval Research, Department of the Navy, Washington, DC (1978).

INITIAL DISTRIBUTION LIST

- | | | |
|----|---|---|
| 1. | Defense Technical Information Center
8725 John J. Kingman Rd., STE 0944
Ft. Belvoir, Virginia 22060-6218 | 2 |
| 2. | Dudley Knox Library
Naval Postgraduate School
411 Dyer Rd.
Monterey, California 93943-5101 | 2 |
| 3. | Dr. Anthony A. Atchley, Chairman PH
Physics Department
Naval Postgraduate School
Monterey, California 93943-5002 | 1 |
| 4. | Dr. D. D. Cleary, Code PH/CL
Physics Department
Naval Postgraduate School
Monterey, California 93943-5002 | 4 |
| 5. | Dr. S.Gnanalingam, Code PH/GM
Physics Department
Naval Postgraduate School
Monterey, California 93943-5002 | 1 |
| 6. | LT Erik O. Johnson
592 Belden Ave.
Camarillo, CA 93010 | 2 |